Università degli studi di Padova

Corso di Laurea Magistrale in Medicina e Chirurgia

Dipartimento Salute della Donna e del Bambino

Direttore: Ch.mo Prof. Eugenio Baraldi

U.O.C. Cardiologia Pediatrica

Direttore: Ch.mo Prof. Giovanni Di Salvo

TESI DI LAUREA:

Multimodality imaging and functional assessment in patients with systemic right ventricle and biventricular physiology: the role of echocardiography

Relatore: Ch.mo Prof. Giovanni Di Salvo

Correlatrice: Dott.ssa Martina Avesani

Laureanda: Anna Molinaroli

Anno Accademico 2023/2024

SUMMARY

ABBREVIATIONS

CHDs: congenital heart diseases

RV: right ventricle

LV: left ventricle

sRV: systemic right ventricle

D-TGA: dextro transposition of the great arteries

cc-TGA: congenitally corrected transposition of the great arteries

ACHD: adult with congenital heart disease

Echo: echocardiography

CMR: cardiac magnetic resonance

CPET: cardiopulmonary exercise testing

eRV-EDA: echocardiographic derived right ventricle end diastolic area

eRV-ESA: echocardiographic derived right ventricle end systolic area

eESA-sA: echocardiographic derived systemic atrium end systolic area

FAC: fractional area change

TAPSE: tricuspid annular plane systolic excursion

eRV-GLS: echocardiographic derived right ventricle global longitudinal strain

sA: systemic atrium

sAS: systemic atrium peak systolic strain

eRV-EDV: echocardiographic derived right ventricle end diastolic volume

eRV-ESV: echocardiographic derived right ventricle end systolic volume

eRV-EF: echocardiographic derived right ventricle ejection fraction

cRV-EDV: CMR derived right ventricle end diastolic volume

cRV-ESV: CMR derived right ventricle end systolic volume

cRV-EF: CMR derived right ventricle ejection fraction

cRV-GLSendo: CMR derived right ventricle endocardial longitudinal strain

cRV-GLSmyo: CMR derived right ventricle myocardial longitudinal strain

ABSTRACT

Background: Systemic right ventricle (sRV) dysfunction is common in patients with ccTGA and D-TGA s/p Mustard/Senning, often leading to early mortality from heart failure. Therefore, a close follow-up of affected patients is crucial to identify early markers of cardiac dysfunction. Currently, standardized protocols for the assessment of sRV dysfunction are lacking.

Purpose: The aim of the study is to compare standard and advanced echocardiographic parameters with CMR-derived parameters in patients with sRV and biventricular physiology and to evaluate their correlation with clinical variables and exercise capacity.

Methods: Patients with cc-TGA and D-TGA after Mustard/Senning who underwent standard and advanced (speckle tracking and 3D) echocardiography and CMR (including feature-speckle tracking) between September 2022 and September 2023 were included. Clinical, imaging parameters and data derived from cardiopulmonary exercise testing (CPET) were collected.

Results: 19 patients were included, median age at CMR was 28 years (IQR 17,25-33). Echocardiographic derived sRV areas correlated with 3D echocardiographic derived sRV volumes (r 0,6, p 0,006 for diastole; r 0,8, p 0,002 for systole). 3D ejection fraction (EF) correlated with FAC and TAPSE (r 0,8, p 0,001 and r 0,7, p 0,03). sRV GLS correlated with systemic atrial strain (sAS) (r -0.6, p 0.01). CMR-derived EF correlated with CMR-derived GLS both endocardial and myocardial (r -0.7, p 0.007; r -0,6, p 0,005). sRV areas as assessed by echo correlated with CMR-derived volumes (r 0.9, p 0.0001 for diastole, r 0.8, p 0.0001 for systole). Similarly, a correlation was found between sRV echo-derived GLS and CMR-derived GLS both endocardial and myocardial (r 0.8, p 0.001; r 0,7, p 0,01 respectively). The only imaging parameter that correlated with peak VO_2 was sAS (r 0,55, p 0.04). When comparing cc-TGA and D-TGA s/p Mustard/Senning, the former showed better GLS-derived values as assessed by CMR (cRV-GLSendo -23.2% vs -17.2%, p 0.002; cRV-GLSmyo -21.2% vs -16.7%; p 0.05), bigger systemic atrial area (20.2 cm^2/m^2 vs 8.4 cm^2/m^2, p 0.005) and higher TAPSE values (16.2 mm vs 12.2 mm, p 0.04).

Conclusions: Echocardiography is a valid tool to assess sRV dimension and function and to guide timing for CMR. The investigation of atrial deformation

imaging may help to better understand diastolic function and the correlation between sAS and peak VO2 may suggest a major role of diastolic function in determining exercise capacity in patients with sRV. Our study also demonstrated that patients with cc-TGA exhibit better cardiac function compared to those with D-TGA after atrial switch.

RIASSUNTO

Introduzione: La disfunzione del ventricolo destro sistemico (sRV) è comune nei pazienti con ccTGA e D-TGA s/p Mustard/Senning e spesso determina mortalità precoce per insufficienza cardiaca. Pertanto, è fondamentale un attento follow-up dei pazienti colpiti per identificare precocemente marker di disfunzione cardiaca. Attualmente, mancano protocolli standardizzati per la valutazione della disfunzione del sRV.

Scopo: Lo scopo dello studio è confrontare parametri ecocardiografici standard e avanzati con parametri derivati dalla CMR in pazienti con sRV e fisiologia biventricolare e di valutare la correlazione tra i parametri di imaging, le variabili cliniche e la capacità di esercizio.

Materiali e metodi: Sono stati inclusi pazienti con cc-TGA e D-TGA corretta con switch atriale che hanno eseguito un'ecocardiografia standard e avanzata (speckle tracking e 3D) e CMR (incluso il feature-speckle tracking) tra Settembre 2022 e Settembre 2023. Sono stati raccolti parametri clinici, di imaging e dati ricavati dal test da sforzo cardiopolmonare (CPET).

Risultati: Sono stati inclusi nello studio 19 pazienti, l'età mediana alla CMR era di 28 anni (IQR 17,25-33). Le aree del sRV calcolate con l'ecocardiografia risultano correlate con i volumi ecocardiografici 3D del sRV (r 0,6, p 0,006 per la diastole; r 0,8, p 0,002 per la sistole). Inoltre, la frazione di eiezione (EF) del sRV è correlata con la FAC e con il TAPSE (r 0,8, p 0,001 e r 0,7, p 0,03). Il GLS del sRV è correlato con lo strain atriale sistemico (sAS) (r -0,6, p 0,01). La frazione di eiezione (EF) calcolata alla CMR correla con il GLS del sRV calcolato alla CMR sia endocardico che miocardico (r -0,7, p 0,007; r -0,6, p 0,005). Le aree del sRV valutate tramite ecocardiografia sono correlate con i volumi calcolati alla CMR (r 0,9, p 0,0001 per la diastole; r 0,8, p 0,0001 per la sistole). Allo stesso modo, è stata trovata una correlazione tra il GLS del sRV calcolato con l'echo e il GLS calcolato alla CMR sia endocardico che miocardico (r 0,8, p 0,001; r 0,7, p 0,01 rispettivamente). L'unico parametro di imaging correlato con il massimo consumo di ossigeno (peak VO_2) è stato lo sAS (r 0,55, p 0,04). Nel confronto tra i pazienti con cc-TGA e quelli con D-TGA, i primi hanno mostrato migliori valori di GLS calcolato alla CMR (cRV-GLSendo -23,2% vs -17,2%, p 0,002; cRV-GLSmyo -

21,2% vs -16,7%, p 0,05), una maggiore area dell'atrio sistemico (20,2 cm^2/m^2 vs 8,4 cm^2/m^2, p 0,005) e valori più elevati di TAPSE (16,2 mm vs 12,2 mm, p 0,04).
Conclusioni: L'ecocardiografia è uno strumento valido per valutare le dimensioni e la funzione del sRV e per determinare il momento più opportuno per eseguire la CMR. Lo studio dello strain dell'atrio sistemico potrebbe contribuire a una migliore comprensione della funzione diastolica; inoltre, la sua correlazione con il massimo consumo di ossigeno al CPET può suggerire un ruolo predominante della funzione diastolica nel determinare la capacità di esercizio. Infine, lo studio evidenzia che i pazienti con cc-TGA mostrano una migliore funzionalità cardiaca rispetto a quelli con D-TGA dopo switch atriale.

1 INTRODUCTION

Advancements in pediatric cardiac diagnostic and surgical methods have led to a significant increase in the adult population affected by congenital heart disease (ACHD). Consequently, the prevalence of CHD within the community has risen substantially and now by far exceeds the number of children with CHD (1). The prevalence of CHD is estimated to be 4 per 1000 adults. These patients often require long-term expert medical care and healthcare-related costs are high. Therefore, the global health burden as a result of CHD increases quickly (2).

1.1 PHYSIOLOGICAL RIGHT VENTRICLE

Improvements in scientific research have recently brought great attention to the right ventricle (RV), often referred to as the "forgotten chamber" due to its overshadowing by its left counterpart (3). The RV differs anatomically and functionally from the left ventricle, making it inappropriate to directly extrapolate our knowledge of left-sided physiopathology to the right heart (4). Imaging the right ventricle with echocardiography is challenging because of its particular crescentic shape, which wraps around the left ventricle. Nevertheless, it is crucial and it should be included as a standard component of echocardiographic examinations of the heart (5).

Historically, the RV was regarded as a passive structure allowing circulation from the body to the lungs. Nowadays it has become evident that the RV is not merely passive, and a deeper understanding of RV morphology and function is essential to elucidate its pathophysiologic mechanism (6).

1.1.1 Embryology

Disparities between the right and left ventricles arise from differences in embryological origins as well as hemodynamic environment (7).

The morphogenesis of the cardiovascular system begins at around 3 weeks of gestation and is mostly completed by 8 weeks in humans. Cells derived from the anterior lateral plate mesoderm coalesce along the ventral midline to form a primitive heart tube. The "first" heart field that forms the heart tube eventually

contributes to specific future chambers: the left ventricle, muscular interventricular septum and atria. On the contrary, the future RV, most of the membranous interventricular septum and outflow tracts derive from cardiac precursors cells in the anterior or “second” heart field (8).

The RV undergoes significant changes with aging, especially after birth and during infancy.

In the embryo and fetus, the RV is the dominant chamber accounting for about 60% of total cardiac output. Additionally, fetal circulation involves parallel ventricular pumping and minimal pressure discrepancy between right and left ventricles, unlike postnatal circulation. At birth, pulmonary vascular resistance decreases rapidly and, by the first postnatal year, RV wall thickness regresses, increasing compliance and leading to normal cardiac morphology with rightward septal convexity (7).

During the embryonic phase, the fetal heart undergoes intricate structural development, continuing to grow in response to changing demands. Myocardial growth predominantly occurs through cellular division until birth, followed by cellular enlargement. Histologically, distinctions in performance and morphology are evident between the two ventricles (9).

The fetal heart exhibits restricted capacity to augment stroke volume, particularly in the right ventricle, as it operates near its functional limits. The regulation of cardiac output involves mechanisms such as the Frank-Starling mechanism and adrenergic stimulation, with heart rate playing a pivotal role in its augmentation (9).

1.1.2 Anatomy

The right ventricle is a thin-walled crescent-shaped structure connected to systemic venous return on one side and to the pulmonary circulation on the other. In normal situ heart, the RV is the most anteriorly positioned chamber, situated directly posterior to the sternum and marking the inferior border of the cardiac silhouette. The interventricular septum forms the left and posterior wall of the RV, typically exhibiting concavity towards the left ventricle, often resulting in the "crescent" shape of the right ventricle on axial cuts (7).

When viewed from the front, the right ventricle takes on a triangular shape, arching over the left ventricle. Starting from the apex, the right edge of the right ventricle appears sharp, forming the acute margin of the heart.

In cross-section, the cavity of the right ventricle resembles a crescent shape. As a result, the curvature of the ventricular septum positions the right ventricular outflow tract anteriorly and superiorly to that of the left ventricle, establishing a distinctive "cross-over" relationship between the outflows of the right and left ventricles (*Figure 1*) (5). This significant spatial arrangement is one of the fundamental prerequisites for sonographers screening for congenital heart malformations as clinically relevant heart malformations such as complete transposition may be present if the outlets lack the "cross-over" sign (5).

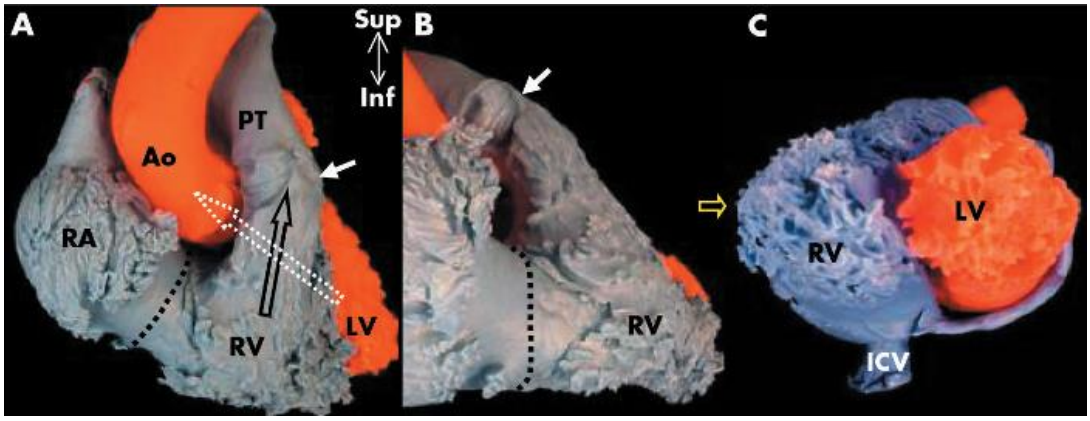

Figure 1- A representation of a normal heart view from different perspectives to display the spatial relationships between cardiac chambers.
Image A: viewed from the anterior aspect, the crossover arrangement between left and right ventricular outflow tracts (dotted arrow and open arrow respectively) is apparent. The pulmonary valve (solid arrow) is situated most superiorly.
Image B: this view from right and anterior shows the triangular shape of the right ventricle delimited by the tricuspid (dotted line) and pulmonary (arrow) valves.
Image C: viewed from the apex, the right ventricle is crescentic, wrapping round the left ventricle (5).

The RV wall is about 2-5 mm in thickness and 25 ± 5g/m^2 in weight. Compared to the left ventricle it has one-third to one sixth smaller mass, it contains 30% more collagen, and its cardiomyocytes are 15% smaller. It is adapted to the high-compliance, low-resistance pulmonary circuit (10).
In the normal RV, two myofiber layers are present: the deep subendocardial layer consisting primarily of longitudinally aligned fibers from base to apex, and the subepicardial layer (approximately 25% of wall thickness) consisting of

circumferentially oriented fibers parallel to the atrioventricular groove that extend from one ventricle to another (*Figure 2*). The circumferential superficial fibers turn obliquely as they extend toward the apex of the heart and continue into the left ventricle (LV) (7). As a result, the right and left ventricles are closely connected not only by the septum but also by shared epicardial myocytes and the pericardial space. These anatomical features form the basis for biventricular functional systolic and diastolic interdependence (11).

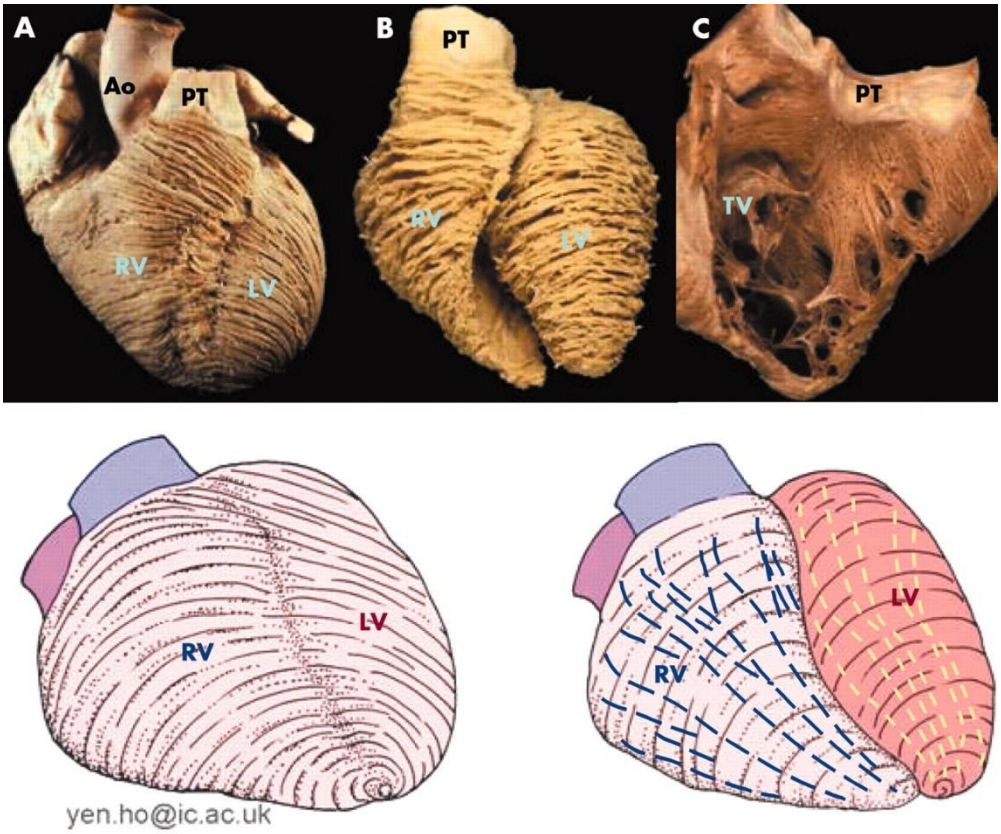

Figure 2- Upper panels: (A) A normal heart viewed from the front shows the circumferential to oblique arrangement of the myofibres in the subepicardium. (B) Myofibres lying deeper than the subepicardium retain the circumferential arrangement in the right ventricle but change from oblique to circumferential in the left ventricle. (C) The right ventricle is opened to show the longitudinally arranged subendocardial myofibres.

The lower panels depict the subepicardial myofibres (left hand panel) and the deeper myofibres (right hand panel) in the ventricles of the normal heart (12).

The RV interior is heavily trabeculated, aside from the regions directly underneath the septal leaflets of the tricuspid and pulmonary valves.

From an anatomical standpoint the RV is more often described in terms of a three-component cavity, according to Goor and Lillehi classification (10), (13) (*Figure 3*):

- The inlet portion contains the tricuspid valvular apparatus (tricuspid valve, chordae tendineae and 3 or more papillary muscles).
- The trabeculated apical myocardium consists of numerous intersecting muscle bundles, running between the parietal and septal wall. Prominent structure arising from these trabeculations include the parietal band, moderator band and septomarginal trabeculation. This layer is relatively thin, making this section more susceptible to increased wall stress.
- The outlet portion comprises the infundibulum or conus, which corresponds to the smooth myocardial outflow region supporting the pulmonary valve leaflets. The size of the infundibulum is independent of the general size of RV and accounts for approximately 20% of the end-diastolic volume in the normal RV (14).

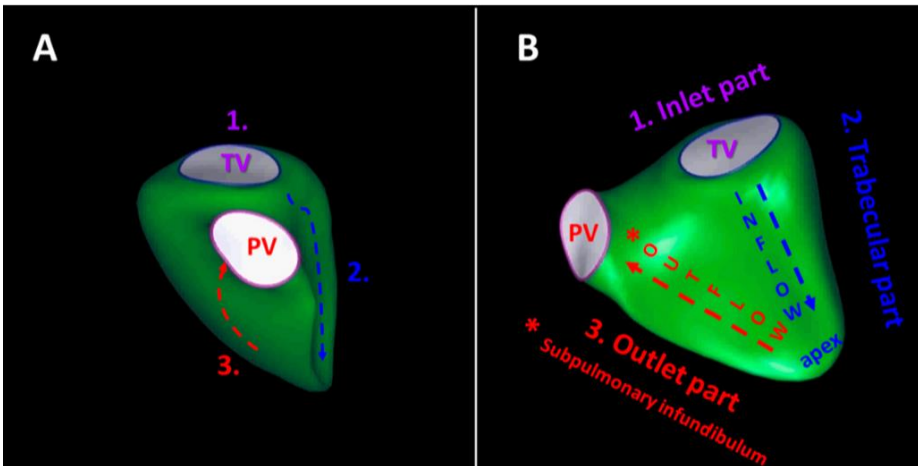

Figure 3- Schematic illustration of the right ventricular components (1.,2.,3.) from anterior (panel A) and septal (panel B) perspectives.

The inlet part (1.) constitutes the tricuspid valve apparatus, the trabecular part (2.) involves the apex with the three intracavitary muscle bands and the outlet part (3.) includes the subpulmonary infundibulum (*) (10).

Although the RV is typically located on the right side of the heart and interfaces with the pulmonary circulation, the anatomic RV is defined by its structural characteristics rather than by its position or connections.

The morphological features that best differentiate anatomic RV include the following (15):

- the presence of coarse trabeculations
- the presence of a moderator band
- the presence of more than 3 papillary muscles
- the trileaflet configuration of the tricuspid valve with septal papillary attachments
- the more apical hinge line of the septal leaflet of the tricuspid valve relative to the anterior leaflet of the mitral valve
- the lack of fibrous continuity between its inlet and outflow valves, as opposed to the aortomitral continuity of the LV.

1.1.3 Contraction pattern

The RV and LV serve different purposes and as such have inherent structural differences, influenced by the two distinct circulatory system they support: pulmonary and systemic, volume-driven and pressure-driven respectively.

The contraction patterns of the two ventricles also differ: the left ventricle exhibits a circumferential contraction pattern with torsional shortening, whereas the RV's contraction pattern is influenced by its complex structure at both macroscopic and microscopic levels (16).

In particular, the RV's structure, consisting of two myofiber layers, results in three primary contributors to RV ejection (16):

1. traction of the tricuspid annulus toward the apex leading to longitudinal shortening.
2. A "bellows"-like inward movement of the RV free wall leading to radial shortening.
3. Traction of the RV free wall associated with left ventricular deformation, leading to anteroposterior shortening.

Therefore, RV function is partly dependent on that of the LV due to ventricular-ventricular interaction along the shared septum (13), (17).

This mechanical coupling of the ventricles is demonstrated by a contribution of the LV to RV pressure generation and vice versa. Specifically, about 20–40% of RV pressure and stroke volume result from LV contraction, indicating a strong ventricular-ventricular interaction (18).

Overall, the contraction of the right ventricle involves a peristalsis-like motion, starting earlier within the inlet and trabeculated myocardium and ending with the contraction of the outlet myocardium, which serves as a pressure buffer while transmitting blood flow to the pulmonary artery (10).
The RV also has a mildly hypokinetic segment consisting on the infundibulum (the conal septum), which does not contribute to contraction in systole (19).

1.1.4 Perfusion

At rest, coronary blood flow and conductance are reduced in the RV compared to the LV. RV coronary flow occurs during both systole and diastole. Due to its thinner wall and greater reliance on coronary perfusion pressure, the RV's perfusion is more susceptible to increases in RV cavity pressure and systemic hypotension. Oxygen consumption and extraction at rest are also lower in the RV than in the LV, leading to a higher oxygen extraction reserve (7). Evidence suggests that pressure-flow autoregulation may be somewhat impaired in the RV. Consequently, during exercise, the RV increases oxygen consumption by increasing oxygen extraction rather than coronary flow (20).

1.2 SYSTEMIC RIGHT VENTRICLE IN CHDs

In a typical, healthy heart, the left ventricle acts as the main pump for the systemic circulation, distributing oxygen-rich blood to the entire body, while the right ventricle acts as the primary pump for the pulmonary circulation, directing deoxygenated blood to the lungs.

However, in certain congenital heart defects, the normal roles of the ventricles are reversed, resulting in a condition known as a systemic right ventricle (sRV): the RV supports high-pressure systemic circulation while the LV supports low-pressure pulmonary circulation (4).

In these conditions the right ventricular dysfunction is the consequence of right ventricle pressure overload. The RV wall is thinner and less muscular compared to the left ventricular wall, resulting in greater distensibility and capacity of the right ventricle, leading to better adaptation to volume overload rather than pressure overload (16).

Management of the morphological right ventricle supporting the systemic circulation remains an ongoing challenge, as sRV dysfunction may lead to a high burden of morbidity and premature mortality from heart failure across all patients, regardless of their underlying cardiac morphology (6).

When the right ventricle, typically designed to support the low-pressure pulmonary circulation, is placed in the systemic position, it must undergo various adaptive mechanisms to effectively handle the increased systemic load. The sRV stands out as a unique model within the anatomical spectrum, characterized by varied short- and long-term adaptations, clinical phenotypes, and prognoses. The guarded prognosis of the sRV compared with the systemic left ventricle is multifactorial, including distinct fibromuscular architecture, shape and function, coronary artery supply mismatch, intrinsic abnormalities of the tricuspid valve, intrinsic or acquired conduction abnormalities, and varied sRV adaptation to pressure or volume overload (6).

It is estimated that conditions involving the sRV account for approximately 10% to 12% of all congenital heart defects and may be encountered in both two-ventricle and single-ventricle arrangements.

Biventricular versions of systemic right ventricle include those patients with congenitally corrected transposition of the great arteries (ccTGA) and complete transposition of the great arteries (D-TGA) treated with an atrial switch operation.
Single ventricle configuration is encountered in patients born with a sRV without a functional LV, including hypoplastic left heart syndrome spectrum and double inlet right ventricle.
In this dissertation we will focus only on sRV and biventricular circulation.

1.3 D-TGA: DEXTRO TRANSPOSITION OF THE GREAT ARTERIES

The transposition of great arteries was first described by Mathew Baillie in 1797; however, the term transposition was only applied in 1814, by Farre, meaning that aorta and pulmonary trunk were placed (positio) across (trans) the ventricular septum (21).

D-TGA represents the second most common cyanotic congenital heart defect, it represents 5-7% of all congenital heart diseases, corresponding to a prevalence of 0,2 per 1000 live births worldwide (22). There is a male predominance with a male/female sex ratio that varies in the literature, from 1,5:1 to 3,2:1 (23).

Familial occurrence exists but is very rare. The exact aetiology of this disease is still unknown; however, some associated risk factors can only explain a small minority of TGA cases. Postulated risk factors include gestational diabetes mellitus, maternal exposure to rodenticides or herbicides and maternal use of antiepileptic drugs. Furthermore, mutations in the growth differentiation factor-I gene, the thyroid hormone receptor-associated protein-2 gene and the gene encoding the cryptic protein have been shown implicated in discordant ventriculo-arterial connections (21).

Overall, the detailed developmental aspects of abnormal ventriculo-arterial relationships remain largely unknown.

1.3.1 Physiology

In complete TGA, also labelled as D-TGA, the “D-” refers to the dextroposition of the bulboventricular loop (e.g. the position of the RV, which is on the right side).

The heart develops as a linear tube made up of several segments: the truncus arteriosus (future aorta and pulmonary artery), bulbus cordis (future infundibulum and aortic vestibule), primitive ventricle, primitive atrium, and sinus venosus. At approximately 5 weeks of gestation, the tube bends to the right (D-loop), positioning the bulbus cordis to the right of the left ventricle. Neural crest mesenchymal cells form two ridges in the bulbus and truncus, which fuse by 6 weeks to form the aortopulmonary septum with a 180° spiral course. This causes the pulmonary artery to twist around the aorta, aligning it with the right ventricle, while the aorta aligns with the left ventricle (24). The main stages of heart development leading to its physiological structure are illustrated in *Figure 4*.

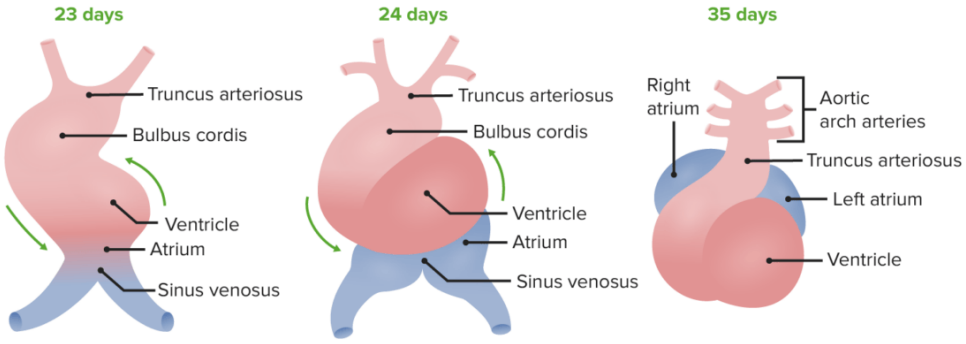

Figure 4- Schematic representations of main stages of heart development.

Anomalies in this spiral septation can lead to dextro transposition of the great arteries. Other hypothesis suggest that TGA occurs due to the disproportionate growth of the subaortic conus and the resorption of the subpulmonary conus, reversing the normal process. This results in the aorta being positioned anteriorly and to the right of the pulmonary artery (25).

As depicted in *Figure 5* D-TGA is characterized by atrio-ventricular concordance and ventriculo-arterial discordance. This arrangement results in the aorta originating from the morphological right ventricle, while the pulmonary artery arises from the left ventricle. The aorta also tends to be on the right and anterior, resulting in the great arteries being parallel rather than crossing as they do in the normal heart (6).

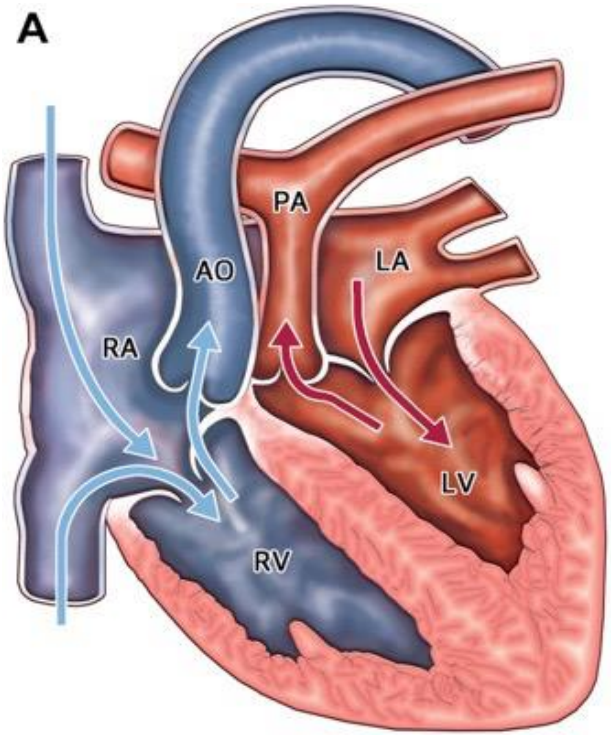

Figure 5- Schematic representation of D-TGA.
(RA - Right Atrium; RV - Right Ventricle; PA - Pulmonary Artery; LA - Left Atrium; LV - Left Ventricle; AO– Aorta)

The result of this condition is that pulmonary and systemic circulations run in parallel as opposed to series. As such, oxygenated blood circulates through a closed circuit involving the lungs and the left cardiac chambers. On the other hand, systemic blood flow is supplied by a separate closed circuit that originates and terminates in the right cardiac chambers (21).

Because the systemic and pulmonary circulations run in parallel, there must be a communication between the two to support life. These connections allow systemic blood to enter the pulmonary circulation for oxygenation and enable oxygenated blood from the pulmonary circuit to enter the systemic circulation, facilitating vital oxygen exchange (26).

The systemic and pulmonary arterial oxygen saturations are thus dependent on one or more of the following anatomic paths for this exchange: intracardiac (patent foramen ovale, atrial septal defect -ASD-, ventricular septal defect -VSD-) and extracardiac (persisting ductus arteriosus -PDA-, bronchopulmonary collateral circulation).

Therefore, the right ventricle, which is not designed to handle systemic pressures, becomes the systemic pump.

In 50% of the cases, the ventriculoarterial discordance is an isolated finding, not associated with other congenital anomalies; in this case D-TGA is called simple. In contrast, D-TGA is termed complex when associated with anomalies such as ventricular septal defect (45%), left ventricular outflow tract obstruction -LVOTO- (25%) and aortic coarctation -CoA- (5%).
The long-term outcome of complex TGA is worse than that of simple TGA, regardless of the type of surgical repair.

1.3.2 Clinical presentation

The natural history of complete transposition of the great arteries is extremely poor and survival to adult life without surgical repair is the exception. Cyanosis, hypoxemic deterioration or heart failure with early death typically characterize the clinical course of untreated infant with complete TGA. The clinical manifestations and course are primarily influenced by the extent of intercirculatory mixing, which depends on several anatomic and functional factors that can be integrated into a useful clinical classification.
In cases where the ventricular septum remains intact, infants typically present with cyanosis within the first day of life. If circulatory mixing occurs through a patent ductus arteriosus, the physiological closure of the ductus can lead to sudden cyanosis and clinical deterioration.
Therefore, in cases of prenatal diagnosis of transposition of the great arteries, a palliative approach is often employed. This may involve treatment with prostaglandin E1 to keep the ductus arteriosus open, or alternatively, the patient may undergo a percutaneous Rashkind atrial balloon septostomy to create a long lasting adequate interatrial communication. These measures can significantly improve oxygenation temporarily until definitive surgery can be performed (21).
Nearly all adult patients with this defect have undergone prior reparative cardiac surgery, although individuals with a large ventricular septal defect and pulmonary vascular disease may sometimes survive with Eisenmenger physiology (26).
Indeed, if there are no obstructive abnormalities and a significant ventricular septal defect exists, facilitating effective mixing between the circulations, cyanosis may

remain undetected except during moments of crying or agitation. Instead, symptoms of congestive heart failure become prominent due to increased workload on the ventricles. Symptoms such as tachypnea, tachycardia, diaphoresis, poor weight gain, a gallop rhythm, and eventually hepatomegaly can be then detected later on during infancy (21).

1.3.3 Treatment

Until the late 1950s, the prognosis for patients with TGA was poor; with 55%, 85%, and 90% mortality at 1 month, 6 months, and 1 year (27). A significant improvement in survival was achieved with the introduction in 1957 of the atrial switch operation by Ake Senning, later refined by William Mustard in 1963 (28).

This procedure involves redirecting the blood flow by creating a two-way baffle within the atria to reroute the oxygenated blood coming from the lungs to the systemic circulation and the deoxygenated blood from the body to the pulmonary circulation.

In the Senning repair, the atrial baffle is fashioned in place using tissue from the right atrial wall and interatrial septum. In contrast, in the Mustard operation, after most of the atrial septum is excised, the baffle is constructed from autologous pericardial tissue or, rarely, synthetic material (*Figure 6*) (29).

Both the Senning and Mustard procedures redirect blood flow at the atrial level. Although the atrial switch provides physiologic correction of the circulation, normal anatomic relationships of the aorta and pulmonary artery are not restored, leaving the morphological RV responsible for supporting the systemic circulation.

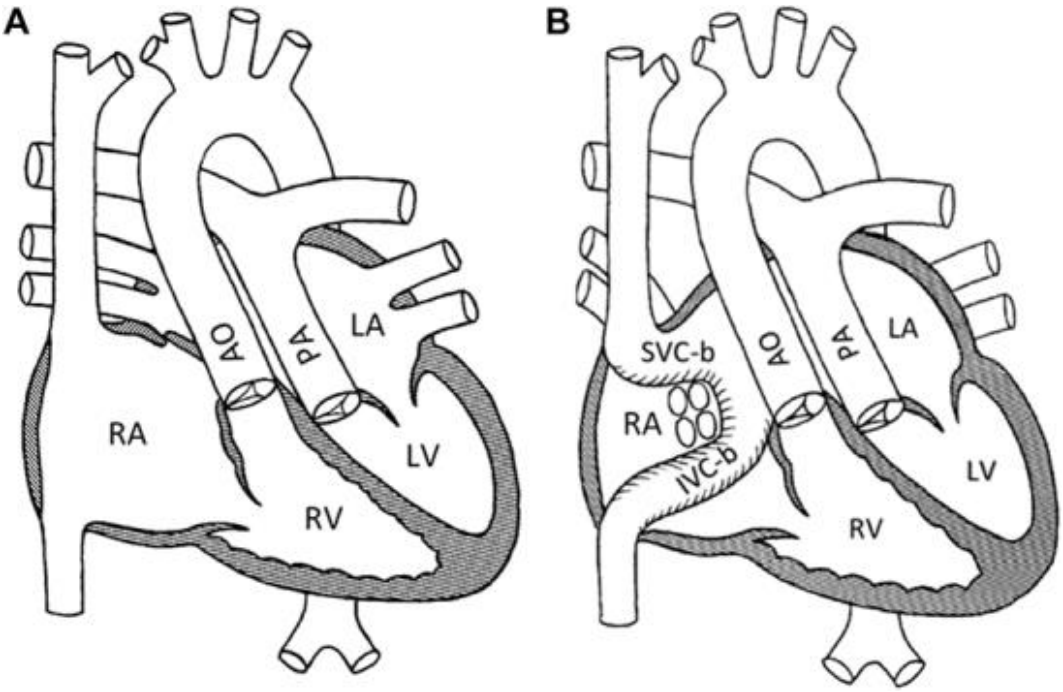

Figure 6- Diagram depicting D-TGA cardiac anatomy before (A) and after (B) Mustard repair. Systemic blood is redirected to the LA via the SVC-b and IVC-b. Meanwhile, pulmonary blood is redirected to the RA via a pulmonary baffle.
(AO = aorta; LA = left atrium; LV = left ventricle; PA = pulmonary artery; RA = right atrium; RV = right ventricle; IVC-b = inferior vena cava baffle; SVC-b = superior vena cava baffle).

Although Mustard and Senning atrial switch procedures have been widely accepted and successful over the past four decades, the quest for an operation to restore the great arteries to their normal ventricular connections continued (30). Starting in 1954, numerous innovative procedures to achieve an anatomic correction were described, but clinical success was not achieved until 1975 by Jatene et al.
Since the 1990s, the preferred surgical therapy for D-TGA has been the arterial switch operation, which is associated with a lower complication rate and a better long-term outcome. This operation restores the normal anatomic arrangement of the circulation and thus represent a more favorable physiological long-term option.

Complex TGAs, characterized by ventricular septal defects and pulmonary stenosis, are often operated upon using a Rastelli-type repair, which combines intraventricular repair with the placement of an extracardiac conduit from the right ventricle to the pulmonary artery. The Rastelli repair has been considered the most

appropriate operation for TGA with large VSD and extensive LVOTO as it achieves complete bypass of the LVOTO and anatomical correction of the transposition pathology (31). Variants of the Rastelli technique, such as the “reparation a l’etage ventriculaire” and Nikaidoh techniques, operate on the same principle. However, further discussion of these surgical techniques is beyond the scope of this dissertation.

Nevertheless, despite the development of new surgical protocols for the treatment of patients with D-TGA, there remains a significant population of young adults who underwent Senning/Mustard repair and continue to require follow-up (32). Atrial redirection surgery remained the primary palliative treatment for patients diagnosed with D-TGA for over 30 years. Survival rates are estimated to be 76% by 20 years of age with mean age at death being 27 years (6), (33). Although no registry exists, it is estimated that at least 3500 patients with D-TGA s/p atrial switch are alive today (34).

1.3.4 Outcomes

In the last decades, advancements in medical and surgical care have significantly improved the long-term survival of patients following atrial switch repair, leading to a higher incidence of long-term complications. These complications include (6), (27), (35):

- Systemic RV dysfunction
- Systemic atrioventricular valve dysfunction
- Arrhythmias
- Baffle stenosis/leaks
- Pulmonary hypertension (≤ 7%)
- Left ventricular outflow tract obstruction (LVOTO)
- Clinical deterioration under specific conditions such as pregnancy.

It is important to recognize that conditions such as pregnancy may be well tolerated initially; however, pregnancy imposes an increased and persistent hemodynamic burden, posing a risk of sRV failure, which may be irreversible.

The long-term complications encountered after atrial switch operation are summarized in *Figure 7*.

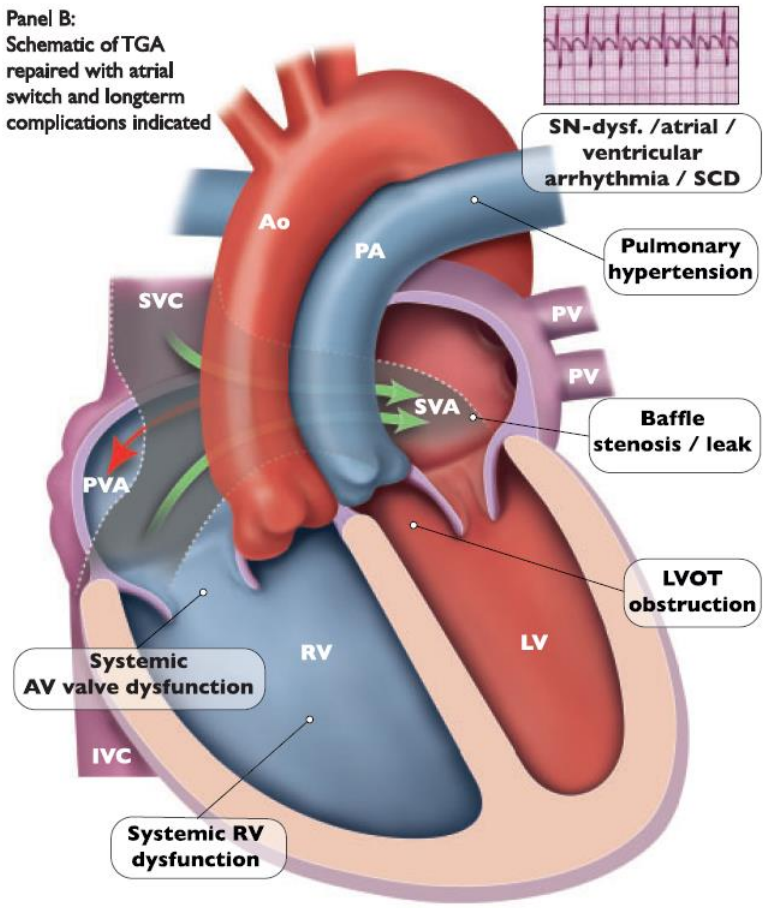

Figure 7- Schematic representation of D-TGA repaired with atrial switch operation and long-term complications to address during follow-up.
(Ao = aorta; AV = atrioventricular; IVC = inferior caval vein; LA = left atrium; LV = left ventricle; LVOT = left ventricular (subpulmonary) outflow tract; PS = pulmonary stenosis (supravalvular/pulmonary artery branch); PV = pulmonary vein; PVA = pulmonary venous atrium; RA = right atrium; RV = right ventricle; SCD = sudden cardiac death; SN-dysf. = sinus node dysfunction; SVA = systemic venous atrium; SVC = superior vena cava; TV = tricuspid valve) (4).

Arrhythmias and sudden cardiac death are the most common major events during young adulthood, while pulmonary hypertension and heart failure-related death become more prevalent after the age of 40 years.

These late sequelae arise because the RV, which typically supports the low-pressure pulmonary circulation, undergoes compensatory remodelling when positioned subaortically to accommodate chronic pressure overload. However, due to its intrinsic structural and contractile properties, the sRV does not ensure long-term performance (27).

1.3.4.1 Systemic RV dysfunction

sRV dysfunction can develop at any stage, but it is typically observed in older patients, suggesting that the anatomic RV is unable to sustain the systemic circulation in the long term. In patients with D-TGA following atrial switch operation, asymptomatic sRV dysfunction usually arises by the third decade of life, with over 50% of patients showing clear signs of heart failure (HF) by their fourth or fifth decade (27).

The dysfunction primarily stems from increased pressure in the RV, leading to ventricular hypertrophy, subsequent dilatation, dysfunction and eventual HF with significant long-term morbidity and mortality. There are multiple factors at play in this scenario, including (6), (35):

- excessive ventricular hypertrophy not matched by normal right coronary supply, potentially leading to myocardial fibrosis.
- Impaired atrio-ventricular transport due to rigid atrial baffles.
- Increased myocardial fibrosis associated with ventricular dysfunction.
- Propensity for arrhythmia.
- Progressive tricuspid regurgitation.
- Associated cardiac lesion or residual lesions after palliation.

These aspects will be further explored in paragraph 1.5.

1.3.4.2 Systemic AV valve dysfunction

Tricuspid regurgitation (TR) arises from both intrinsic abnormalities of the tricuspid valve (more common in cc-TGA patients), and the effects of systemic right ventricle (sRV) dilatation and consequent annular enlargement. As mentioned earlier, the sRV is poorly suited to function as a high-pressure ventricle, leading to

sRV dilatation and secondary TR. This creates a vicious circle where TR exacerbates ventricular and annular dilation, further worsening TR (27).

1.3.4.3 Arrhythmias

Bradyarrhythmia, tachyarrhythmia and sudden cardiac death (SCD) are common and potentially devastating late complications.

Bradycardia and chronotropic incompetence are due to the loss of sinus rhythm, while atrio-ventricular conduction typically remains intact. Sinus node dysfunction seems to be caused by damage to sinus node/atrial conduction tissue or interruption of sinus node blood flow at the time of surgery (6).

Interatrial reentry tachycardia (IART), the most prevalent type of tachycardia, is associated with natural conduction barriers, such as fibrosis related to suture lines and patches within the native right atrium. Unlike typical atrial flutter in the normal heart, IART is usually slower, with a commonly observed 2:1 atrioventricular relationship, which may result in asymptomatic presentation. However, malignant tachycardias associated with a history of supraventricular tachycardia can lead to sudden cardiac death (6).

High heart rates are often poorly tolerated haemodynamically due to the inability to increase preload, a consequence of the restrictive atrial baffles (33).

1.3.4.4 Baffle complications

The majority of late reinterventions are attributed to venous baffle complications, which include baffle leaks, stenosis or both. Baffle leaks occur in over two-thirds of patients, while stenosis affects approximately 10% of patients.

The superior vena cava arm of the baffle is particularly susceptible to obstruction, especially when a transvenous pacemaker or intracardiac defibrillator lead is present. Typically, these conditions can be managed conservatively, unless peripheral edema and hepatic congestion develop (31).

Baffle leakage can result in either systemic-to-pulmonary shunting, leading to pulmonary overflow, or pulmonary-to-systemic shunting in the presence of distal flow obstruction. This can manifest with cyanosis or paradoxical embolism (29).

1.3.4.5 Pulmonary arterial hypertension

Pulmonary arterial hypertension (PAH), characterized by an elevated mean pulmonary arterial pressure exceeding 25 mmHg at rest, is a significant complication documented in up to 7% of patients who survive to adulthood following atrial switch repairs. PAH leads to a reduction in functional capacity and overall quality of life.

The aetiology of PAH in D-TGA may be related to many factors including repair performed after the age of 2 years, pre-repair shunts at the ventricular or great artery level, and obstruction of the pulmonary venous baffle. Patients with mild elevation of pulmonary pressure during early post-operative catheterization are at an increased risk for developing PAH (36).

1.3.4.6 LVOTO: left ventricular outflow tract obstruction

LVOTO stands for "left ventricular outflow tract obstruction," a condition characterized by an obstruction to the blood flow as it exits the left ventricle. This obstruction often arises from the bulging of the interventricular septum towards the low-pressure subpulmonic left ventricle and it is frequently associated with systolic anterior motion of the mitral valve (4).

1.4 ccTGA: CONGENITALLY CORRECTED TRANSPOSITION OF THE GREAT ARTERIES

Described by Von Rokitansky in 1875, congenitally corrected transposition of the great arteries (ccTGA) is a rare congenital heart defect, with an estimated prevalence of 1 per 33.000 live births, accounting for approximately only 0,05% of all congenital heart defects (37). Situs solitus is typically observed, with the apex of the heart usually remaining leftward, although the cardiac position is often more mesocardic than usual. Dextrocardia occurs in about 20% of the cases, while 5% of patients with ccTGA exhibit situs inversus. Population-based studies continue to suggest the potential significance of environmental factors in the aetiology of this condition (38).

1.4.1 Physiology

This condition is characterized by a combination of atrio-ventricular and ventriculo-arterial discordance.

Morphogenetically, the primitive cardiac tube, anchored at one end by the sinus venosus and at the other end by the truncus arteriosus, loops to the left (L-looped) rather than to the right (D-looped) as in the normal heart (*Figure 8*) (39).

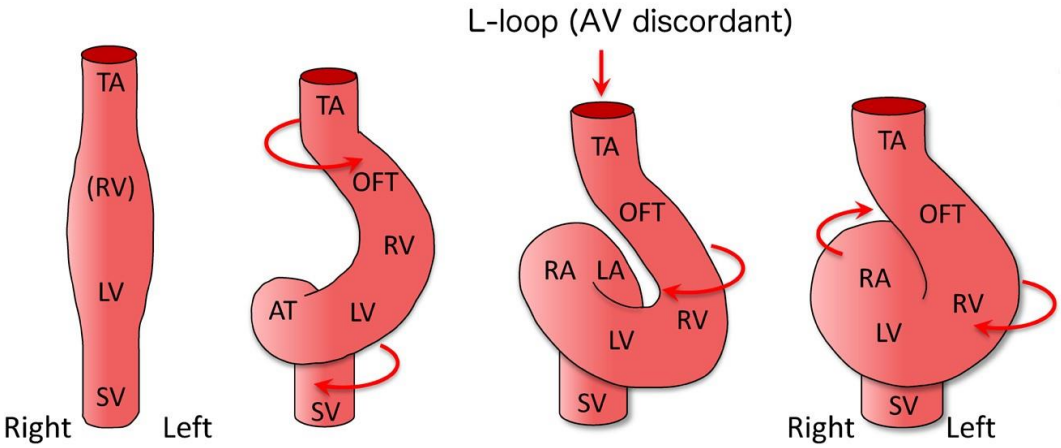

Figure 8- L-cardiac loop in atrioventricular discordance.

(TA= truncus arteriosus; RV= right ventricle; LV= left ventricle; AT= atrium; SV= single ventricle; OFT= outflow tract)

This abnormal cardiac looping results in the morphologic left ventricle being positioned to the right and the morphologic RV to the left, in association with a transposed ventriculo-arterial connection(39).

Hence, in patients with ccTGA, situs solitus and normal atrial arrangement, the systemic venous return joins the morphologic right atrium. This atrium is connected by a mitral valve with the morphologic left ventricle, which, in turn, supports a discordantly connected, transposed pulmonary artery. The left atrium, receiving the pulmonary veins, connects through a tricuspid valve with the morphologic right ventricle, which in turn supports a transposed aorta, positioned anterior and leftward of the pulmonary artery. Once again, the right ventricle assumes the role of a systemic pump (*Figure 9*).

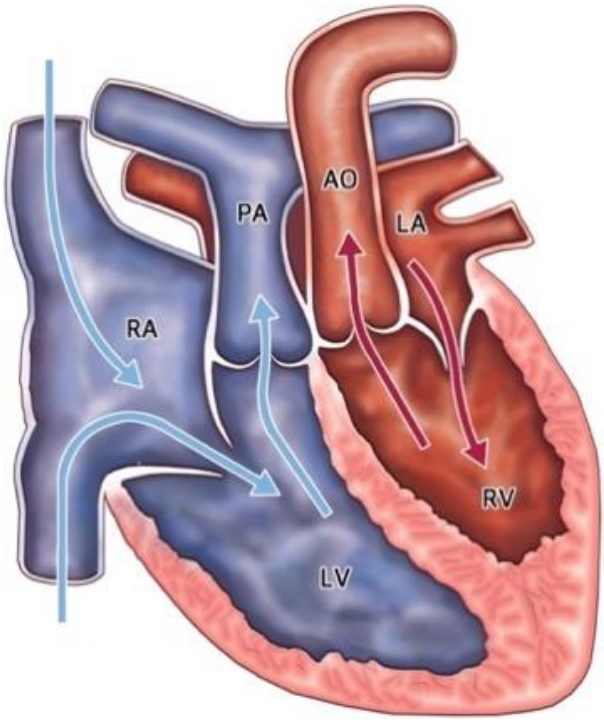

Figure 9- Schematic representation of cc-TGA.

(RA= Right Atrium; RV= Right Ventricle; PA= Pulmonary Artery; LA= Left Atrium; LV= Left Ventricle; AO= Aorta)

The majority of patients with ccTGA, approximately 80%, have associated lesions. The most common ones include (6):

- ventricular septal defect
- pulmonary stenosis
- Ebstein anomaly of tricuspid valve. This anomaly results in systemic atrio-ventricular valve regurgitation and sRV volume overload. This condition may progress due to ventricular dilatation and sRV dysfunction. Timely surgery, involving valve replacement, is crucial for preventing sRV failure and improving prognosis in ccTGA
- abnormalities of the conduction system, which predispose patients to complete heart block.

1.4.2 Clinical presentation

The natural progression and clinical presentation of ccTGA are heavily influenced by associated malformations, with the timing and severity of symptoms in childhood often reflecting the presence of these associated lesions.

Most patients with isolated ccTGA do not display symptoms during childhood and rarely experience complications until adulthood, remaining undiagnosed up to the ninth decade. Consequently, it is highly likely that some people with ccTGA are never diagnosed, making it difficult to ascertain its true prevalence. Life expectancy is significantly reduced compared to the general population, with the majority of patients progressing to cardiac failure by the fourth or fifth decade of life (40).

On the contrary, when associated lesions are present, clinical presentation tends to occur earlier.

Infants with ccTGA may come to attention with bradycardia, with or without heart failure, indicating high-degree atrioventricular block, tachyarrhythmia, cyanosis due to inadequate pulmonary blood flow, and/or congestive heart failure (40). Congestive heart failure may be indicative of a cardiac arrhythmia, but more commonly suggests the presence of a large ventricular septal defect, dysplasia or displacement of the left-sided tricuspid valve with regurgitation, obstructive anomalies of the aortic arch, or a combination of these anomalies (41).

1.4.3 Outcomes

ccTGA is characterized by a slowly progressive pathophysiology, which despite excellent early survival rates, carries a significant risk of long-term complications related to systemic RV dysfunction, tricuspid regurgitation and arrhythmias. Heart failure and sudden cardiac death are the two leading causes of death in patients with ccTGA (18). Huhta et al. demonstrated that sudden cardiac death accounted for 40% on ccTGA deaths (42). However, heart failure tends to develop in older patients, as shown in a study by Hauser et al. where all subjects younger than 35 years were symptom free with normal systolic ventricular function (43).

Systemic RV dysfunction in cc-TGA is usually associated with severity of tricuspid valve regurgitation, which typically precedes the onset of clinical heart failure. Patients with isolated cc-TGA with minimal tricuspid regurgitation may maintain preserved ventricular function for decades (18).

Additionally, cc-TGA patients are more susceptible to developing complete heart block and reentry tachyarrhythmias due to the more anteriorly placed atrioventricular node and elongated atriventricular bundle (18).

1.5 FAILING SYSTEMIC RIGHT VENTRICLE

The natural history of patients with ccTGA and D-TGA after atrial switch procedure is characterized by long-term sRV dysfunction and the development of heart failure, arrhythmias, and sudden cardiac death (7), (27).

Heart failure occurs when the cardiac output fails to match the body's metabolic demands, stemming from structural or functional impairment of ventricular filling or ejection. The majority of heart failure research focuses on failing left ventricle and for a long time right ventricular function has been considered as simply a transferring chamber, where the cardiac output would remain unaffected by its exclusion (44), (45).

Right heart failure is defined as impaired RV contractility resulting from myocardial dysfunction, elevated pressures or volume overload. Its true prevalence is challenging to estimate, and it is not currently divided into stages as with the left counterpart.

Despite significant progresses in understanding risk factors for adverse outcomes in transposition of the great arteries, there are substantial challenges due to the distinct morphologic and physiologic differences between the right and left ventricles. This limits the ability to directly apply knowledge gained from the evaluation and management of heart failure in the non-congenital heart disease population to individuals with TGA (44).

In this patients, systemic RV dysfunction can develop at any stage and it is almost uniformly present in older patients, indicating that the morphological RV is unable to sustain the systemic circulation in the long run (46), (47).

Individuals with sRV and biventricular circulation may experience RV failure due to various factors including anatomical differences, altered pressure-volume loops, associated tricuspid valve disease, or rigid atrial baffles after atrial switch procedures (18).

Patients in this group show evidence of RV failure before the symptoms start and when those develop, they are strong predictors of mortality. For this reason, earlier identification of adult patients who are starting to develop sRV failure may improve clinical outcomes by enabling closer monitoring and the timely initiation of advanced therapies, before the development of end-organ dysfunction (45).

The exact mechanisms leading to sRV failure are not fully understood but likely involve a combination of factors.

As previously described, the right and left ventricle have evolved to fulfil different inherent functions. In a physiologic situation, RV serves as a low-pressure pump and its function is heavily influenced by favourable loading conditions, with its contractility sensitive to afterload changes. RV pressure-volume loop differs from that of the LV, exhibiting a trapezoidal shape reflecting distinct contraction and relaxation patterns.

On the other hand, when the anatomic RV is placed in the systemic position, several pathophysiologic adaptations must occur.

Increased afterload leads to the systemic right ventricle adopting a pressure-volume loop similar in shape to that of the left ventricle and results in compensatory RV dilation to maintain stroke volume (18). Specifically, Theissen et al. found that the systemic RV has a higher end-diastolic volume than a systemic LV, indicating greater dilation of the RV under systemic pressure (48).

The RV dilatation leads to increase in myocardial wall stress and oxygen demand: the thin-walled RV becomes hypertrophied, resulting in increased RV end-diastolic pressure. This hypertrophy also restricts right coronary artery perfusion to the diastolic phase, whereas it is normally present throughout the entire cardiac cycle (18).

Unfortunately, with disease progression, this compensatory mechanism fails, causing further RV dilation and resulting in reduced cardiac output.

Multiple studies have demonstrated that the sRV likely functions with a lower baseline ejection fraction than the LV. Both Connelly and Benson et al. demonstrated that in both cc-TGA as well as atrial switch patients the RV has a lower resting EF than the LV (49), (50).

In conclusion, many factors, including myocardial fibrosis, impaired coronary reserve, tricuspid regurgitation-induced volume overload, arrhythmias, and chronotropic incompetence may contribute to ventricular dysfunction and heart failure in individuals with a systemic right ventricle.

Figure 10 provides a comprehensive summary of all these aspects. Each aspect will be discussed in detail the following paragraphs.

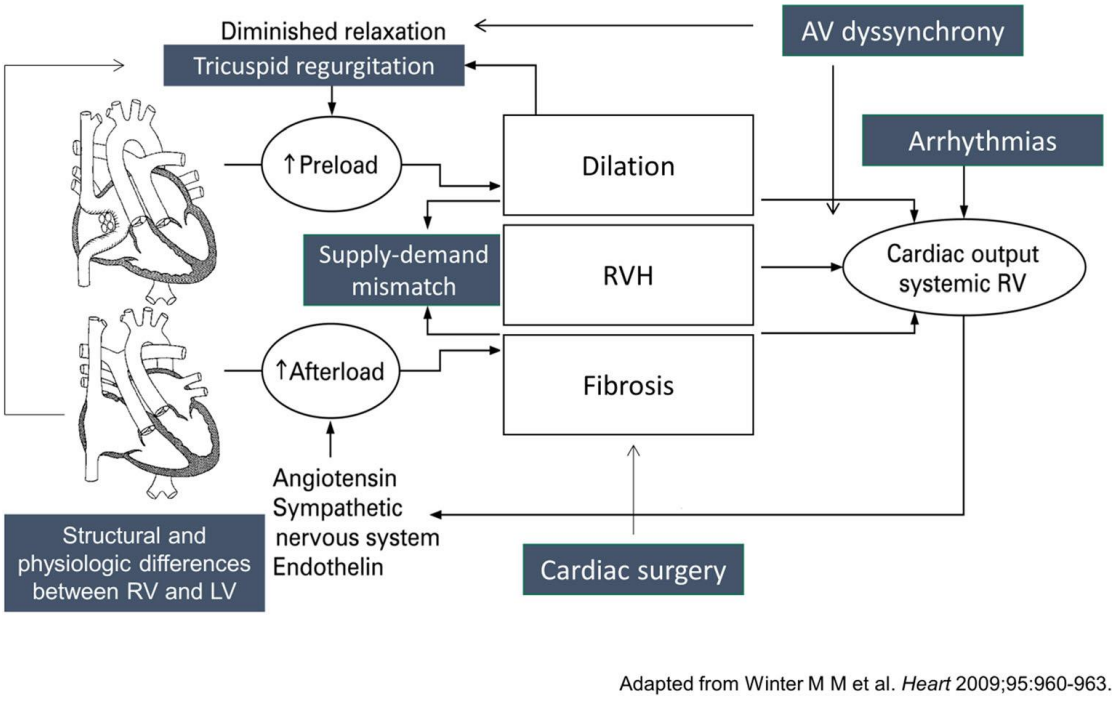

Figure 10- Mechanism of sRV failure (18).

1.5.1 Myocardial fibrosis

Studies utilizing MRI have shown that late gadolinium enhancement (LGE), indicative of fibrosis, is common in patients with sRV, correlating with functional deterioration such as increased sRV end-systolic volume index and decreased sRV ejection fraction. Moreover, the presence of LGE has been validated as a prognostic marker for new onset arrhythmia and heart failure (49).

Babu-Narayan et al. in a single-center study of 36 patients, described late gadolinium RV enhancement in 61% of patients and showed that it was correlated with age, ventricular dysfunction, electrophysiological parameters and adverse clinical events (50).

Mechanisms contributing to fibrosis include preoperative hypoxemia, inadequate coronary supply and increased RV wall stress (18).

1.5.2 Impaired coronary reserve

Patients with sRV are more prone to develop myocardial ischemia. They are characterized by a unique circulatory physiology that leads to chronic pressure overload and compensatory sRV hypertrophy. Since perfusion of the sRV is maintained mainly by the right coronary artery, coronary artery supply in hypertrophic and dilated sRV may be inadequate for the myocardial needs, especially at stages of high demand (18). The mismatch could be responsible for fibrosis development, myocardial injury and systolic dysfunction.

Nejc Pavsic et al. demonstrated an interplay between myocardial ischemia and myocardial disfunction in adult patients with sRV (51). Assessment of myocardial ischemia is anyway difficult due to complex anatomy and diagnostic accuracy would be improved only through hybrid imaging tecniques.

1.5.3 Tricuspid regurgitation

Tricuspid valve itself is often dysplastic in patients with sRV, causing tricuspid regurgitation (TR).

However, TR in sRV is also the consequence of different mechanisms.

Firstly, TV annulus dilation and the consequent valvar leaflet tethering due to RV dilation under chronic systemic pressure, as well as the traction of the septal leaflet due to right-to-left septal shift, are considered to be some of the main causes of TR in patients with sRV (52).

Secondly, the mismatch between the increased oxygen demand of the subvalvular apparatus due to papillary muscle hypertrophy and multifactorial reduced coronary flow reserve may contribute to worsening valvular dysfunction.

By now, it is not clearly elucidated whether the TR is cause or consequence of failing sRV, anyway it is well established that TR increases ventricular and annular dilation which, in turn, worsens TR is a vicious circle (53). Therefore, whether TR is causative or a secondary complication remains speculative.

Prieto et al. found that morphological anomalies of the TV are better predictors of TR severity in ccTGA than sRV dilation, which seems secondary, suggesting a major role of tricuspid anatomical malformations (54).

1.5.4 Conduction disorders

Conduction disorders and heart block requiring ventricular pacing are extremely common in ccTGA. Indeed, they are found in up to 50% of patients with ccTGA, and ventricular pacing is required in almost 50% of them in adult life. Chronic LV pacing may induce pacemaker-related dyssynchrony worsening sRV dilation and failure, as well as TR (41).

Furthermore, as previously mentioned, the atrial switch surgery for D-TGA may damage the sinoatrial node/atrial conduction tissue or temporarily decrease blood flow to the sinoatrial node, causing post-operative sinus node dysfunction. Atrial arrhythmia related to surgical scars or atrial dilation due to valve regurgitation can induce a tachycardia-mediated cardiomyopathy and exacerbate ischaemia and cardiac events (55).

1.5.5 Chronotropic incompetence

Chronotropic incompetence refers to the inability of the heart to appropriately increase its heart rate in response to physiological demands such as exercise or stress. It is demonstrated that during exercise testing, oxygen consumption is lower in both symptomatic and asymptomatic patients with sRV compared to those with systemic LV (56). Chronotropic incompetence is more pronounced in cc-TGA than in patients following atrial switch, the aetiology of which remains unclear (56).

1.6 ASSESSMENT OF sRV DYSFUNCTION

Recent advancements in cardiac imaging have brought significant attention to the right ventricle, highlighting its importance in cardiac physiology. (57). The nature of previous surgery and other intervention is highly variable rendering each patient unique.

Despite excellent survival rates into adulthood for both D-TGA and ccTGA, the natural progression of these cardiac conditions is characterized by progressive and inevitable sRV dysfunction, leading to heart failure, exercise intolerance, arrhythmias and premature death in early adulthood (58).

Imaging in adult with congenital heart disease (ACHD) must be preceded by a thorough clinical evaluation including a detailed patient's history, review of previous surgical procedures or other interventions and physical examination. A comprehensive understanding of congenital cardiac anatomy, terminology, pathophysiology, and past procedures is essential for optimal ACHD imaging and interpretation.

Data obtained by the different imaging modalities should be integrated with functional assessment, particularly cardiopulmonary exercise testing, which has shown strong prognostic value in ACHD patients (59). Furthermore, due to the frequent occurrence of arrhythmic events, it is crucial to have regular follow-up with Holter ECG. In certain cases, extended ECG monitoring might also be necessary. (47).

Cardiovascular imaging has shifted from a single modality approach to an integrated multimodality-based approach in order to achieve a comprehensive assessment of individual patient morphology, pathophysiology, and haemodynamic, as well as to guide therapy.

Developing lesion-specific imaging protocols for follow-up studies is recommended to ensure that crucial information for clinical decision-making are included; furthermore, it facilitates longitudinal data comparison (59).

Overall, ACHD patients would benefit from a multimodality imaging approach, with the selection of imaging modalities based on the specific clinical question and with consideration for minimizing risk to the patient (59).

Figure 11 provides a summary of the use of multimodality imaging for assessing RV function.

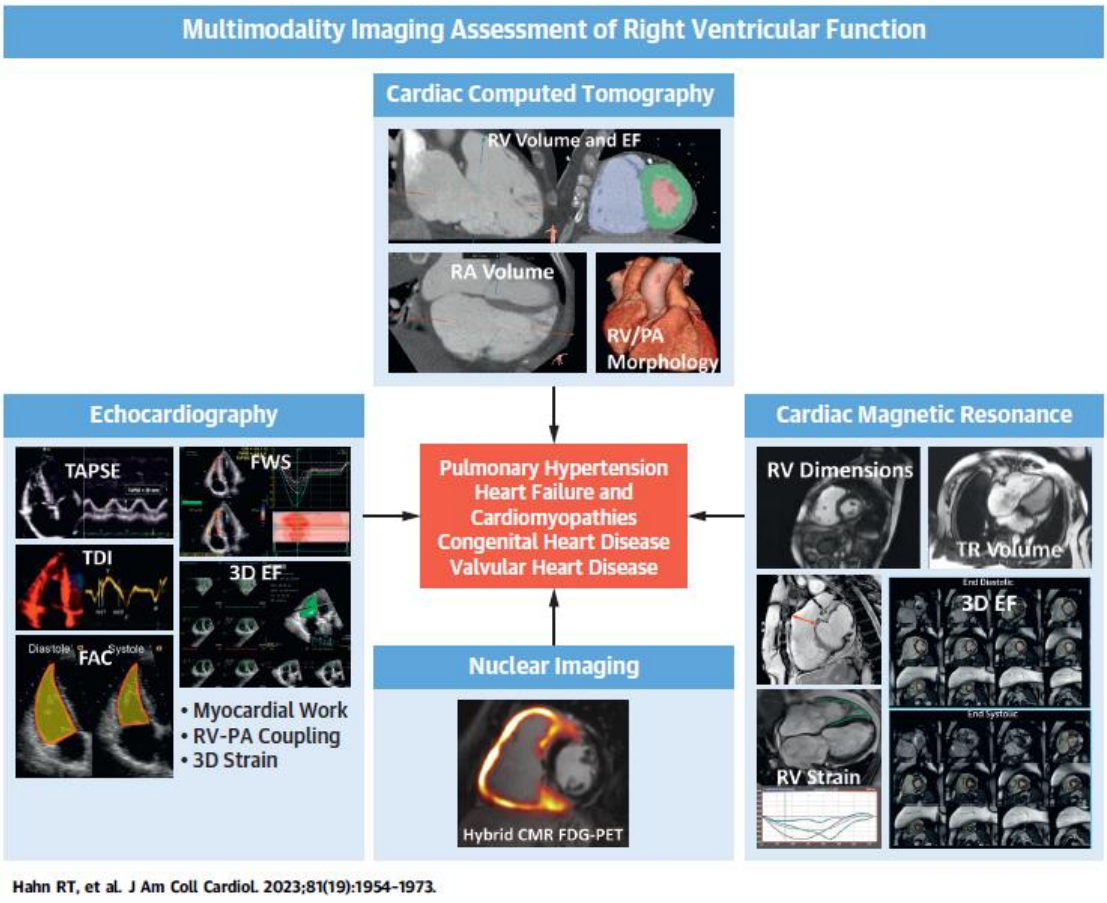

Figure 11- Multimodality imaging of right heart function (57).

This dissertation will focus on the roles of the echocardiography and cardiac magnetic resonance (CMR) in the follow up of patients with sRV and biventricular physiology.

1.7 ROLE OF ECHOCARDIOGRAPHY IN THE ASSESSMENT OF sRV

Echocardiography remains the primary imaging modality for routine assessment of adults with systemic right ventricle. It allows simultaneous morphological, hemodynamic, and functional analysis of the right heart in a single examination (60), (61), (62).

However, due to the asymmetrical, crescent shape and position of the right heart behind the sternum, comprehensive evaluation of the right ventricle requires imaging from different echocardiographic windows and multiple imaging planes using various echocardiographic modalities (57).

Unlike the standardized methods for assessing left ventricular function, there is no uniform approach for evaluating right ventricular function (3).

It is important, therefore, for echocardiographers to remember that none of the following variables are sufficiently accurate to be used alone. A combination of indices should be taken into account before concluding about the level of RV dysfunction.

Furthermore, in patients with limited echocardiographic windows, additional imaging techniques will be required and selected according to the clinical question.

Limitations to echocardiography in D-TGA and cc-TGA include the evaluation of the systemic right ventricle and baffle patency following atrial switch procedure because of poor acoustic window.

1.7.1 Assessment of sRV systolic function

The echocardiographic evaluation of RV systolic function can be performed qualitatively and quantitatively, using two- and three-dimensional methods, as well as regional and global assessment (63). However, assessing RV ejection fraction (eRV-EF) quantitatively can be challenging due to the complex RV geometry, resulting in subjective evaluations. Therefore, a range of echocardiographic variables has been developed to evaluate RV systolic function.

To this regard tricuspid annular plane systolic excursion (TAPSE), pulsed doppler S wave (S’), fractional area change (FAC) and global longitudinal strain (eRV-GLS) are, by far, considered the most valuable in clinical practice for evaluating right ventricular systolic function. Therefore, it is recommended that at least one of

these parameters should be routinely reported when assessing RV systolic function (57), (63).

In the following paragraphs, the main echocardiographic parameters for assessing right ventricular systolic function will be analysed.

1.7.1.1 TAPSE

Tricuspid Annular Plane Systolic Excursion (TAPSE) is a method used to measure the systolic excursion of the RV annular segment along its longitudinal plane, typically from a standard apical 4-chamber window (64). This measurement reflects the longitudinal function of the right ventricle. It is generally understood that the greater the descent of the base in systole, the better the RV systolic function. This approach to examinate the longitudinal myocardial fibers through TAPSE measurement is based on the anatomical theory that most of the right ventricular myocardial fibers originate from the heart's apex and insert into the right atrioventricular junction, resulting in a majority of longitudinally oriented fibers in the right ventricle (60).

The normal range of TAPSE value is approximately 24 ± 3,5 mm; while a value below 17 mm is considered abnormal (65). Derik et al. showed that sRV long-axis function was notably reduced compared with that of either the normal subpolmonary right ventricle or the systemic left ventricle, probably as a consequence of the longitudinally arranged myocardial fibers adapting to chronic increased afterload (66).

1.7.1.2 Tissue Doppler-derived right ventricular systolic excursion velocity S'

Tissue doppler imaging (TDI) is an echocardiographic technique that uses doppler principles to measure the velocity of myocardial motion. TDI can be performed in pulsed-wave and colour modes.

In clinical practice, this technique is employed to assess the velocity of the tricuspid annulus and the basal free wall segment of the right ventricle, as these regions are considered to provide the most reliable and reproducible measurements. Conversely, assessing the mid and apical ventricular free wall velocities is typically discouraged during routine echocardiographic studies, due to the lower likelihood of obtaining adequate signals and higher variability in measurements (64).

Specifically, Tissue Doppler systolic excursion velocity (TDI S') of the tricuspid annulus is a reproducible and easily obtainable measure of longitudinal right ventricular systolic performance, similar to TAPSE (67). Normal values of TDI S' are 14,1 ± 2,3 cm/s and values < 9,5 cm/s is associated with global right ventricular dysfunction (65).

1.7.1.3 FAC: fractional area change

Fractional area change (FAC) is calculated from RV end-diastolic and end-systolic areas. It is assumed to be an indicator of global RV systolic function and it has been demonstrated to correlate with RV EF measured by magnetic resonance imaging (64). A reduced RV FAC, typically defined as < 35%, reflects lower RV systolic function (10). This parameter is considered to be more accurate for assessing RV function compared to TAPSE.

1.7.1.4 GLS: global longitudinal strain

Global longitudinal strain (GLS) represents the percentage change in myocardial deformation compared with its original length: lengthening and thickening result in a positive value; while shortening and thinning result in a negative value. On the other hand, its derivative, strain rate (SR), represents the rate of myocardial deformation over time and it is expressed as $second^{-1}$ (67). Strain rate has demonstrated a strong correlation with myocardial contractility in both vitro and vivo experimental settings (64). Strain and SR imaging play a crucial role in distinguishing between active and passive myocardial movement, as well as quantifying different aspects of myocardial function, including longitudinal myocardial shortening, which cannot be assessed visually. This comprehensive assessment of myocardial function is particularly relevant when evaluating the sRV, due to its unique hemodynamic conditions.

Strain can be acquired using tissue doppler imaging (TDI) or speckle-tracking echocardiography.

TDI-derived strain and strain rate have several limitations, including angle-dependence, limited spatial resolution and the need of time-consuming steps for data acquisition and processing. For these reasons these measurements are not highly reproducible (60).

Speckle-tracking echocardiography (STE) is a newer technique used to measure strain and strain rate, which tracks movement by monitoring speckles (natural acoustic markers) within the two-dimensional (2D) ultrasound image.

These markers, known as "speckles," are tracked from one frame to another. Specialized software enables spatial and temporal image processing, allowing for the identification and selection of these elements within ultrasound images. The geometric displacement of each speckle reflects local tissue motion. By monitoring these speckles, both strain and strain rate can be computed. One advantage of this approach is that it tracks movement in two dimensions, along the direction of the wall, rather than along the ultrasound beam, making it angle-independent (60).

RV global longitudinal strain assessed by echocardiography (eRV-GLS) has been found to correlate with CMR-derived RV EF (cRV-EF) in patients with sRV and was shown to be impaired in patients compared with controls. Pooled data suggest that global longitudinal RV free wall strain > -20% (< 20% in absolute value) is likely abnormal while normal values are defined with eRV-GLS= -29 ± 4,5 (65). Impaired RV GLS was also shown to be predictive of adverse clinical events in patients with TGA (61).

Finally, studies have demonstrated that systemic right ventricle global longitudinal strain was able to discriminate between D-TGA patients s/p atrial switch with and without a CMR-derived sRV ejection fraction of at least 45% (68).

Figure 12 provides an overview of the echocardiographic parameters used to evaluate right ventricular systolic function.

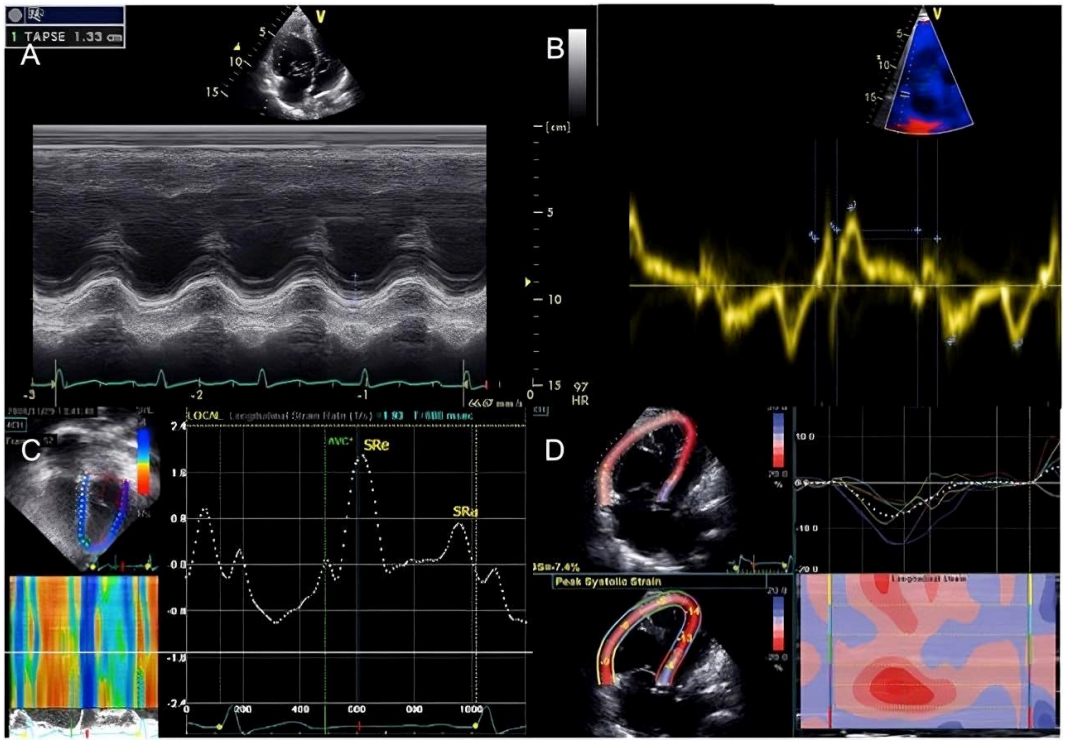

Figure 12- Longitudinal variables commonly used for assessing right ventricular systolic function. Panel A: TAPSE in the lateral apical four-chamber (A4C) view and M-mode. Panel B: TDI-S' in the lateral A4C window. Panel C: TDI-derived strain imaging in the A4C view. Panel D: Two-dimensional strain imaging acquired using speckle-tracking echocardiography in the A4C view (60).

1.7.2 Assessment of sRV diastolic function

The prognosis and exercise capacity of patients with a systemic right ventricle are impacted not only by systolic dysfunction but also by diastolic dysfunction (60).

The non-invasive assessment of right ventricle diastolic function has encountered significant challenges. Applying concepts of left ventricular diastolic function to the right ventricle is challenging due to the different geometry and physiological properties of the two ventricles. Additionally, the lack of standardized methods for assessing right ventricular diastolic function makes early detection more difficult (69). Given the different phases of diastole, assessing ventricular diastolic function requires the inclusion of multiple parameters.

Specifically, systemic right ventricular diastolic function is assessed through Doppler interrogation of the tricuspid inflow, tissue Doppler interrogation of the lateral tricuspid valve annulus and evaluation of the systemic atrium (67).

E-wave deceleration time represents trans-tricuspid flow velocity during early ventricular filling. Conversely, during the late diastolic phase, atrial contraction occurs, and the trans-tricuspid flow velocity is represented by the A-wave. In normal diastolic function, the early filling velocity (E-wave) is higher than the atrial contraction velocity (A-wave) (67). Thus, E/A ratio <0.8 indicates impaired ventricular relaxation, while elevated E/A ratio (>2.1) indicates restrictive physiology, which is a late phase of diastolic dysfunction (65).

Another parameter indicative of right ventricular relaxation is the early diastolic tissue Doppler velocity, known as E'. An increased E/E' ratio (E/E' > 6) indicates elevated right ventricular filling pressures (67).

It is also important to assess systemic atrial size because it can impact sRV diastolic function (69). Additionally, atrial strain measurements for both atria are increasingly used both to gain a better understanding of overall atrial function and because it may be a more sensitive tool for detecting atrial dysfunction in the context of ventricular diastolic dysfunction (70).

In patients with D-TGA post-Mustard/Senning operations, abnormal ventricular filling may result not only from impaired diastolic properties but also from filling abnormalities caused by surgical baffles, which can hinder atrial contraction's ability to enhance ventricular filling (71).

To the best of our knowledge, no studies to date have evaluated atrial strain in patients with a systemic right ventricle and bi-ventricular physiology (D-TGA s/p Mustard-Senning or cc-TGA).

1.7.3 Three-dimensional echocardiography for the assessment of sRV

More contemporary techniques such as three-dimensional (3D) echocardiography offer novel insights into RV function assessment. However, it is important to note that this technique has less validation data compared to traditional metrics (63).

The utilization of three-dimensional echocardiography for evaluating the right ventricle provides numerous advantages compared to the traditional two-dimensional approach. It eliminates errors associated with foreshortening and variability in selecting tomographic planes for measurement.

This method enables a comprehensive evaluation of the entire right ventricle, covering the RV inflow, outflow and apex, as well as the assessment of the right ventricular ejection fraction. Moreover, three-dimensional measurements of size and function closely resemble those obtained via cardiac magnetic resonance imaging, mitigating the limitations of two-dimensional measurements (57).

1.8 ROLE OF CMR IN THE ASSESSMENT OF sRV

Cardiac magnetic resonance imaging (CMR) is the gold standard for quantitative assessment of the RV in many congenital heart diseases (59), (72), (73).

At present, imaging is performed on 1.5 to 3 Tesla systems, along with dedicated cardiac phased-array coils equipped with multiple elements and electrocardiogram triggering for optimal image acquisition. Despite its advantages, CMR has clear limitations, including limited temporal resolution, contraindication in patients with intracardiac devices (which applies to most of our patients) and relatively limited availability. Furthermore, the process of data acquisition and RV analysis are rather time consuming.

The goals of CMR evaluation of D-TGA after atrial switch and ccTGA patients include:

- quantitative evaluation of the size and function of the sRV
- imaging of the systemic and pulmonary venous pathways to identify potential obstruction and/or baffle leak(s)
- assessment of tricuspid valve regurgitation
- evaluation of the left and right ventricular outflow tracts to identify any signs of obstruction
- detection of aortopulmonary collateral vessels and other associated anomalies
- evaluation of the coronary arteries to ensure proper blood supply
- detection of myocardial fibrosis and/or scar tissue that may affect cardiac function.

Overall, CMR plays a crucial role in providing detailed and comprehensive information about systemic right ventricle in patients with congenital heart diseases, helping to guide clinical management and treatment decisions.

1.9 ASSESSMENT OF EXERCISE CAPACITY

Most of patients with sRV and TGA are classified as New York Hear Association (NYHA) functional class I and II, indicating that they are well adapted and report no symptoms despite presence of sRV dilatation and reduced exercise capacity on cardiopulmonary exercise testing (CPET) (74). However, a higher NYHA class is associated with adverse outcomes such as heart failure, sudden cardiac death and arrhythmias.

Patients with sRV and biventricular physiology typically exhibit reduced exercise tolerance due to chronotropic incompetence (75), (76) and a limited capacity to increase stroke volume during exercise (77), (78). Chronotropic response to exercise is an important determinant of exercise capacity, which in turn predicts hospitalization and death over the following year (79), (80). In this setting CPET plays a crucial role in longitudinal follow-up for the serial assessment of exercise capacity and chronotropic incompetence (56). It can also 'unmask' baffle leakage (desaturation) that may not be apparent at rest.

Reduced exercise capacity may be caused by deterioration in systemic right ventricular function overtime. Interestingly, there seems to be no association between resting parameters of sRV systolic function and peak oxygen uptake during CPET (81).

In TGA patients after Mustard operation, a correlation between peak VO2 and quantitative parameters of sRV function (such as TAPSE) measured during stress echocardiography has been observed (82). However, this study is limited by low number of patients included.

Additionally, Goncalves et al. demonstrated that heart rate at anaerobic threshold ≤95 bpm has the highest predictive power of all cardiopulmonary exercise test parameters analysed for heart failure events in TGA patients with systemic circulation supported by the morphological right ventricle (83).

1.10 MANAGEMENT FOR FAILING SYSTEMIC RIGHT VENTRICLE

A growing number of patients with a sRV are reaching adulthood and rational clinical management for this unique physiologically complex population is therefore mandatory (35).

The burden of D-TGA patients with previous atrial switch repair and cc-TGA patients with heart failure will only increase in the coming years due to the aging adult congenital heart disease population and improvements in the management of advanced heart failure (40), (74).

Evidence-based guidelines on pharmacologic treatment of sRV failure have not been established yet. Current medical therapy translated from left heart failure has limited benefit for these patients. To date, drug therapy options in a failing systemic RV is limited and randomized trials are scarce (84), (85), (86). The following section provides an overview of the current state of art regarding the treatment of systemic right ventricular dysfunction.

Aldosterone inhibitors, which have anti-fibrotic potential, have no significant effect on sRV function (87), (88). However, it is important to underline that treatment with aldosterone antagonists has only been investigated in very few studies.

Teun van der Bom et al. in the randomized controlled trial VAL-SERVE suggested a treatment effect of Valsartan in a subgroup of symptomatic patients with sRV, without reduction of sRV EF in the treatment arm while there was a significant reduction in the placebo arm (89).

The use of beta-blockers might have a beneficial role, especially at higher tolerated dose. Nevertheless, the use of beta-blockers is hampered by risk of conduction abnormalities and bradycardia, especially in ccTGA.

Nederend et al. found out that the use of Sacubitril/Valsartan in a cohort of patients with sRV is well tolerated and associated with an improvement in functional capability, discrete amelioration of systolic right heart function and reduction of HF biomarkers (90). Fusco et al. demonstrated that Sacubitril/valsartan reduce mortality and hospitalization in patients affected by sRV and heart failure with reduced ejection fraction (91). In addition, the study documented an improvement in clinical status and cardiac reverse remodelling. This novel drug association could earn a central role in the guideline-directed medical therapy for sRV heart failure.

Patients with sRV and end-stage heart failure should be referred to a transplant centre for advanced mechanical circulatory support devices or heart transplantation. Determining the optimal timing of heart transplant in these patients is difficult because most of the patients seem to be clinically stable for a long time and their hemodynamic deterioration may be unexpected and rapid. Since transplant waiting lists are long and there is high mortality on the waiting list, it seems prudent to refer patients to tertiary centres for mechanical support devices before organ failure and pulmonary hypertension occur.

Mechanical support devices for sRV failure are rather limited. A ventricle assist device can be used as bridge to transplantation or as a destination therapy (27), (55). The number of patients undergoing such treatment is limited, and selecting patients and managing the complications associated with ventricular assist devices remain significant challenges.

2 AIM OF THE STUDY

Congenital practitioners place great emphasis on preventing systemic right ventricle (sRV) failure, making longitudinal follow-up essential to identify markers of cardiac dysfunction and provide appropriate treatment.
While echocardiography remains the primary diagnostic tool, assessing cardiac and tricuspid valve function presents challenges. Cut-off values and quantitative parameters derived from adult recommendations for different cardiac conditions are often used to evaluate sRV function, despite potential inaccuracies. Additionally, obtaining an optimal acoustic window may be difficult in these patients (92).
Although cardiac magnetic resonance imaging (CMR) is considered more reliable for quantitatively assessing sRV volumes and ejection fraction, its use is limited by longer execution times, higher costs, and limited availability (93), (94).

The aim of the study is to compare a comprehensive range of standard and advanced echocardiographic parameters with CMR-derived parameters in patients with a systemic right ventricle and biventricular physiology (ccTGA and D-TGA after Mustard/Senning operations), in order to understand which echocardiographic parameters are most significant in assessing sRV dysfunction.
Furthermore, the study seeks to evaluate the correlation between imaging parameters, clinical variables and exercise capacity.

3 MATERIAL AND METHODS

3.1 STUDY POPULATION

This is a retrospective single centre study, carried out at the Department for Women's and Children's Health of the Padua University Hospital between March and September 2023.

Patients were considered eligible for this study if they met the following criteria:

- had systemic right ventricle and biventricular circulation in D-TGA with previous Mustard or Senning surgery, or in cc-TGA
- had a clinical visit, echocardiography and/or cardiac magnetic resonance scan within one year prior to the last follow-up visit (September 2022-September 2023).

Patients excluded from the study were those implanted with pacemaker, cardioverter defibrillator or any CMR-incompatible device.

3.2 CLINICAL DATA

Patients' records were reviewed from the Galileo's eHealth medical platform of the Padua University Hospital.

Clinical data extracted from medical record included: age, body mass index, body surface area (BSA), New York Heart Association (NYHA) functional class, time since surgery and ongoing medications.

Moreover, data derived from cardiopulmonary exercise test (CPET) done within 12 months from any imaging exam were collected, when available. The following parameters were considered: peak oxygen consumption (VO_2 peak), minute ventilation/carbon dioxide production (VE/VCO_2) slope, metabolic equivalents (METs) and peak respiratory exchange ratio (peak RER).

All data collected were kept confidential and anonymized for statistical analysis. A code and a unique identifier were assigned to each subject to anonymize personal information and prevent it from being traced back to the patient's demographic data.

3.3 CARDIAC RESTING IMAGING

3.3.1 Echocardiographic data

All the echo studies were performed by using Vivid E9 ultrasound system (General Electric Healthcare, Horten, Norway). Standard and advanced transthoracic echocardiographic exams were performed by one experienced pediatric cardiologist (MA).

Chamber quantification measurements were assessed according to the current European Association of Echocardiography guidelines (65).

Global sRV function was visually assessed from the apical four chamber view. The following parameters were calculated:

1. right ventricle end-diastolic and end-systolic area (eRV-EDA, eRV-ESA)
2. fractional area change (FAC)
3. tricuspid annular plane systolic excursion (TAPSE)
4. lateral tricuspid annulus peak systolic velocity (TDI S')
5. tricuspid E/E' ratio
6. tricuspid E/A ratio
7. the presence and the magnitude of the tricuspid regurgitation
8. right ventricle global longitudinal strain (eRV-GLS)
9. systemic atrium peak systolic strain (sAS)
10. systemic atrium end systolic area (eESA-sA)
11. right ventricle end-diastolic and end-systolic volume (eRV-EDV, eRV-ESV) and ejection fraction (eRV-EF)

The ECG trace, obtained by placing three electrodes on the patient's chest, was helpful in identifying the diastolic and systolic phases of the cardiac cycle.

From the apical window we measured: RV end-diastolic and end-systolic area (eRV-EDA, eRV-ESA), and these values were then normalized for BSA (eRV-EDAi, eRV-ESAi).

eRV-EDA (cm^2) and eRV-ESA (cm^2) were obtained delineating the ventricular endocardial border both in systole and diastole from the annulus, along the free wall to the apex, and then back to the annulus, along the interventricular septum. Trabeculation, tricuspid leaflets, and chords were included in the cavity area.

Fractional area change (FAC) was calculated as the percentage of change between the eRV-EDA and eRV-ESA (*Figure 13*).

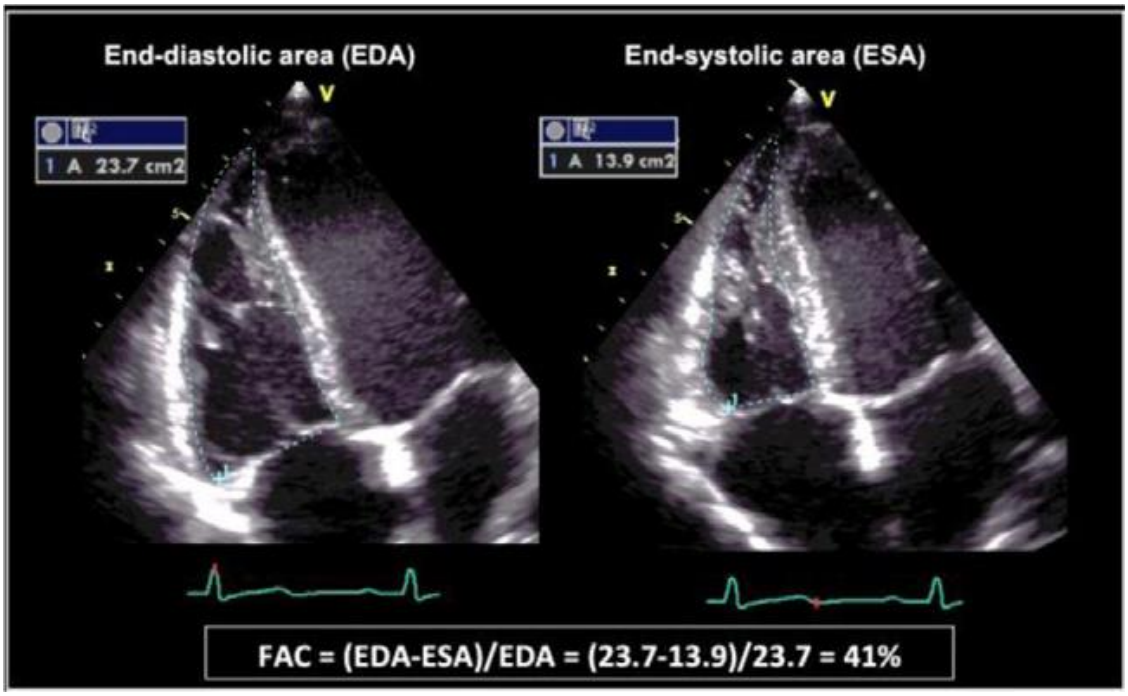

Figure 13- FAC calculation. The image in apical 4-chamber (A4C) view show how the endocardial border is traced to calculate eRV-EDA (A) and eRV-ESA (B). From these values, it is possible to derive the FAC using the formula: 100 x [(eRV-EDA-eRV-ESA) /eRV-EDA] (65).

Tricuspid annular plane systolic excursion: TAPSE (mm) was determined by M-MODE, measured between end-diastole and peak systole, with the cursor aligned along the direction of the lateral tricuspid annulus and measuring the amount of longitudinal motion of the annulus at peak systole (*Figure 14*).

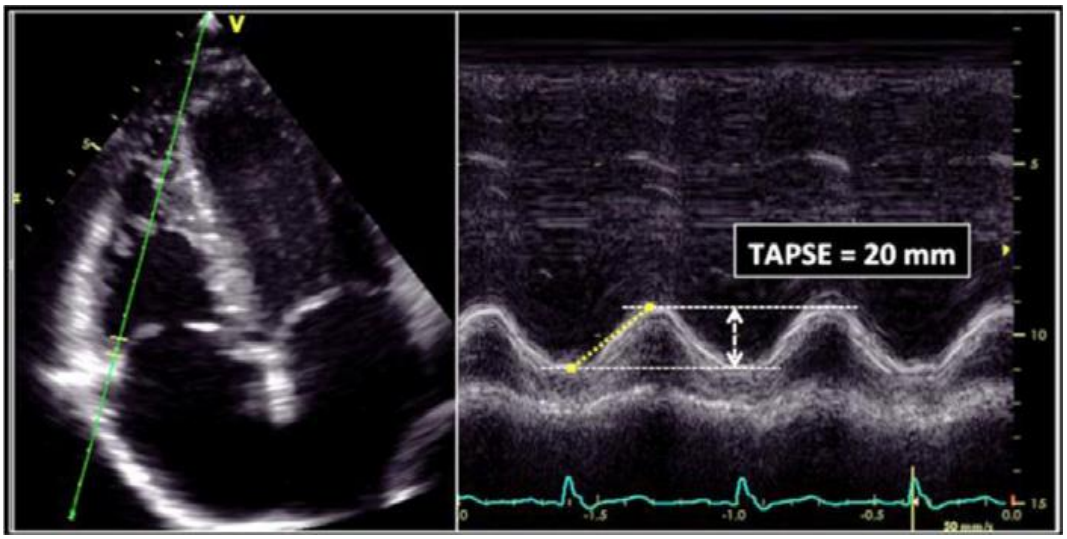

Figure 14- Measurement of tricuspid annular plane systolic excursion (TAPSE) (65).

TDI S' (m/s) was calculated using Pulsed-Wave Tissue Doppler (PW-Doppler), obtained in the view that achieves parallel alignment of the Doppler beam with right ventricle free wall (*Figure 15*).

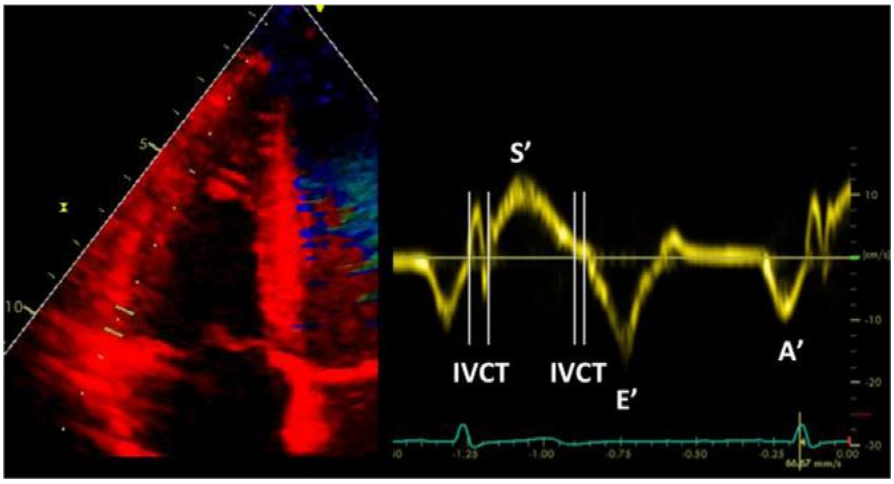

Figure 15- Measurement of TDI S' using PW-Doppler (65).

Tricuspid inflow PW Doppler velocities, lateral wall TDI velocities and the derived E/E' ratio were also assessed. The component parameters of the ratio were obtained using Pulse-Wave Doppler at the tips of the tricuspid valve leaflets and Tissue Pulse-Wave Doppler at the tricuspid valve lateral annulus respectively.

E/A values were calculated using Pulse-Wave Doppler, positioned at the level of the tricuspid valve.

Tricuspid regurgitation was evaluated as none/trivial (0 = single narrow jet), mild (1 = multiple narrow jets), moderate (2 = wide jet reaching the mid part of the atrium) and severe (3 = wide jet reaching the roof of the atrium). The color scale was set at a Nyquist limit of 50–60 cm/s.

Speckle tracking global longitudinal strain (GLS) of the systemic right ventricle, including the RV free wall and septum (eRV-GLS), was determined in the apical four-chamber view on the ultrasound device itself or on an offline workstation (Echo PAC version 112.99, Research Release, GE Healthcare), which allows semi-automated analysis.

The images selected for the speckle tracking analysis had a frame rate between 50 and 100 frames per seconds, with a ≤ 10% variability in heart rate, as already detailed in previous article on speckle tracking echocardiography and congenital heart diseases (95), (96).

After having drawn manually 3 points (2 annular and 1 apical), the software tracked the myocardium semi-automatically throughout the heart cycle. Manual adjustments, if needed, were performed to optimize the region of interest. The automated algorithm allowed global longitudinal strain to be calculated, dividing the right ventricles in 6 segments (*Figure 16*). GLS by speckle tracking was defined as the average peak negative value on the strain curve during the systole. Segments not well visualized were not included, in case of ≥ two non-visualizable segments the patient was not included in the analysis.

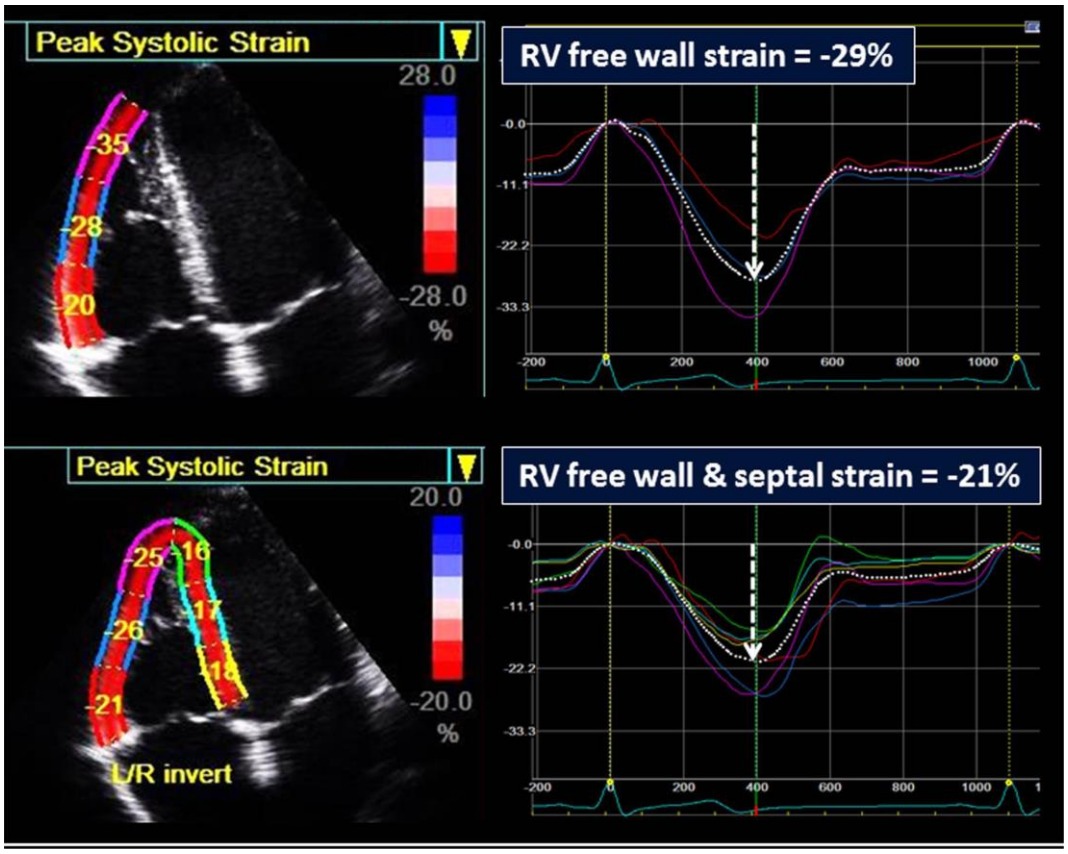

Figure 16- Measurement of RV systolic strain (65).

From the apical four chamber view, the systemic atrium (sA) peak systolic strain (sAS) was also measured. The atrial wall was traced manually (3 points) and adjusted, if necessary, resulting in strain curves from a total of 3 atrial segments. Global peak atrial strain was defined as the average of the maximum positive values during RV systole of the 3 analysed atrial segments.

Systemic atrium end systolic area (eESA-sA) was calculated at end-systole, on the frame just prior to tricuspid valve opening, by tracing the sA blood-tissue interface, excluding the area under the tricuspid valve annulus.

When available, 3D images were elaborated to obtain 3D volumes (eRV-EDV, eRV-ESV) and ejection fraction (eRV-EF).
Afterwards the volumes were indexed for the patients' body surface area (BSA) at the time of the ultrasound.
Finally, we compared Echocardiographic data with parameters derived by CPET.

Analysis of echocardiographic data was blind to CMR results, to clinical data and to CPET findings.

3.3.2 Cardiac Magnetic Resonance data

Each CMR examination was carried out by one pediatric cardiologist experienced in pediatric CMR imaging (ER) and one radiologist (AC) with the same CMR scanner (Achieva 1.5 Tesla, Philips Healthcare; Best, the Netherlands). CMR measurements were performed by the same operator, to empower data consistency and assessment was blind to Echo data.

A standard CMR protocol for evaluating patients with sRV includes: real-time localization imaging in three planes without ECG-gating and during free breathing; cine SSFP sequence with gated-breathing to report anatomy, size of ventricles and function; phase contrast (PC) sequences Qp:Qs; whole-heart isotropic 3D SSFP imaging for vascular evaluation without contrast material administration and visualization of proximal and mid-coronary arteries; LGE imaging along the long and the short axes (97).

In the following study, we evaluated steady-state free precession (SSFP) end-inspiratory breath-hold ECG-gated cine-images in long axis views and a stack of short-axis slices covering the ventricular cavities. Moreover, right ventricular outflow tract (RVOT) obstruction was assessed by specific RVOT view, together with analysis of the superior systemic venous pathways and possible presence of baffle leaks. All patients underwent Gadolinium 0.2 mmol/kg administration to assess the presence of late gadolinium enhancement (LGE) in the 4-chamber and short-axis view.

Image analysis were performed by using Philips Intellispace Cardiovascular post-processing software. The sRV epi- and endocardium were manually segmented in cine short axis on end-diastolic and end- systolic images.

For all patients, sRV end diastolic and systolic volumes (cRV-EDV, cRV-ESV) and sRV ejection fraction (cRV-EF) were acquired, according to the current guidelines (98). Volumes were then indexed for the patients' body surface area (BSA) at the time of the exam (cRV-EDVi, cRV-ESVi).

Myocardial strain was assessed using feature tracking (FT) applied to SSFP cine images during post-processing with a dedicated software (Qstrain, Medis Suite Version 4.0.38.4, Leiden, Netherlands). Global longitudinal strain of the sRV

(cRV-GLSendo, cRV-GLSmyo) was evaluated on long-axis images (99), (100). Initially, the endocardial borders of the sRV were manually segmented in the end-diastolic phase and then automatically expanded to all phases with an automatic border detection algorithm. The endocardial borders were checked for accuracy in all cardiac phases and manually adjusted if necessary. The software provided endocardial peak systolic strain (101), (102).

Finally, we compared CMR data with parameters derived by CPET.

3.4 STATISTICAL ANALYSIS

Baseline characteristics are reported as percentages for categorical variables, as means and standard deviations for continuous variables when normality was verified, and as median and interquartile range (IQR) when normality was not verified by the Kolmogorov–Smirnov test. The Student's t-test for independent samples or the Mann–Whitney test when normality was not verified was used for the analysis of the variables.

Differences between groups for continuous variables were analysed based on distribution using t-test, Kruskal-Wallis test or Wilcoxon-Mann-Whitney test, as appropriate.

The relationship between CMR-derived sRV data, echocardiographic parameters and exercise test results was evaluated using the Pearson and Spearman correlation coefficient as appropriate.

The statistical significance was set at p value <0.05.

Analysis was performed using SPSS statistic software version 22 (IBM SPSS Statistics Version 22, Chicago IL, USA).

4 RESULTS

4.1 PATIENTS

In our institutional medical records, twenty-two patients with sRV and biventricular physiology underwent echocardiography and CMR between September 2022 and September 2023. Both echocardiographic and CMR data were available for 19 patients.

Median age at CMR was 28 years (IQR 17,25-33); 11 (58%) were female.

Eleven had cc-TGA, 4 of them had previous physiologic repair, consisting of large ventricle septum defect closure (3 patients) and atrial septal defect closure (1 patient). Of the 8 patients with D-TGA 5 had undergone Senning repair (63%).

cc-TGA patients were significantly younger than patients with D-TGA (p 0.03; cc-TGA median age 21 years IQR 16,25-28,5; D-TGA median age 32 years IQR 28,25-36,75).

Most patients were clinically asymptomatic.

Cardiopulmonary exercise test (CPET) data were available for 17 out of 19 patients.

Demographic and clinical features of patients are summarized in *Table I*.

Variables	Study cohort (n=19)
Diagnosis	
cc-TGA, n (%)	11 (57,9%)
D-TGA, n (%)	8 (42,1%)
s/p Mustard	3 (37%)
s/p Senning	5 (63%)
Gender	
Female, n (%)	11 (58%)
Male, n (%)	8 (42%)
Age in years at CMR	28 (IQR 17,25-33)
cc-TGA age in years	21 (IQR 16,25-28,5)
D-TGA age in years	32 (IQR 28,25-36,75)
NYHA class ≥ II, n (%)	7 (36,8%)
Ongoing treatment, n (%)	
Beta-blocker	4 (21%)
ACE-I	4 (21%)
Diuretics	2 (10,5%)
Anticoagulants	2 (10,5%)
Antiaggregant	1 (5,2%),
Sacubitril/valsartan	2 (10,5%)
CPET	**Study cohort (n=17)**
Peak VO_2 (ml/kg/min)	24,3 (SD 6,6)
VE/VCO_2 slope	32,6 (SD 3,9)
Peak RER	1,16 (SD 0,1)
METs	12,8 (SD 2,4)

Table I- Demographic and clinical features of the study cohort. Values are mean (SD), median (interquartile range), or n (%).

Legend: CMR: cardiac magnetic resonance, cc-TGA: congenitally corrected transposition of the great arteries, D-TGA: dextro transposition of great arteries, NYHA: New York Heart Association, Peak VO2: peak oxygen consumption, VE: minute ventilation, VCO2: carbon dioxide production, Peak RER: peak respiratory exchange ratio, METs: Metabolic Equivalent of Task.

4.2 CARDIAC IMAGING

Echocardiographic and CMR data were available in 19 patients.

2D speckle tracking echocardiography was available in 15 patients, 3D echocardiography in 11 patients, CMR feature tracking was assessed in 18 performed scans.

TR was assessed as mild in 4 patients (21%), moderate in 13 (68.4%) and severe in 2 (10.5%) patients.

Echocardiographic and CMR variables are summarized in *Table II* and *Table III*.

Echocardiographic variables	**Study cohort (n=19)**
eRV-EDA (cm^2)	31,06 (SD 9,14)
eRV-EDAi (cm^2/m^2)	22,48 (SD 12,38)
eRV-ESA (cm^2)	20,13 (SD 8,61)
eRV-ESAi (cm^2/m^2)	14,24 (SD 8,34)
FAC (%)	37,41 (SD 7,62)
E/A	2 (SD 1,03)
TAPSE (mm)	13,93 (SD 5,24)
S'velocity (cm/s)	9,55 (SD 2,66)
E/E'	12,04 (SD 6,09)
E' velocity (m/s)	0,96 (SD 0,28)
eRV-EDV (ml)	127,18 (SD 40,67)
eRV-EDVi (ml/m^2)	81,32 (SD 32,51)
eRV-ESV (ml)	67,26 (SD 29,55)
eRV-ESVi (ml/m^2)	42,52 (SD 20,15)
eRV-EF (%)	47,44 (SD 8,88)
eRV-GLS (%)	-15,35 (SD 4,02)
eESA_sA (cm^2)	21,50 (SD 12,13)
eESA_sAi (cm^2/m^2)	15,35 (SD 9,87)
sAS (%)	18,17 (SD 7,87)
Moderate-severe TR, n (%)	15 (78,9 %)

Table II- Echo variables analysed in the study. Values are mean (SD) or n (%).

CMR variables	Study cohort (n=19)
cRV-EDV (ml)	170.25 (SD 73.56)
cRV-EDVi (ml/m^2)	104.61 (SD 22.79)
cRV-ESV (ml)	87.22 (SD 39.94)
cRV-ESVi (ml/m^2)	67,72 (SD 61,15)
cRV-EF (%)	50,11 (SD 8,44)
FAC (%)	34.16 (SD 10.45)
cRV-GLSendo	-20.62 (SD 5.35)
cRV-GLSmyo	-19.22 (SD 4.99)

Table III- CMR variables analyzed in the study. Values are mean (SD).

Legend: eRV: echo-derived right ventricle, cRV: CMR-derived right ventricle, EDA: end-diastolic area, ESA: end-systolic area, EDAi: indexed end-diastolic area, ESAi: indexed end-systolic area, FAC: fractional area change, TAPSE: tricuspid annular plane systolic excursion, EDV: end-diastolic volume, ESV: end-systolic volume, EDVi: indexed end-diastolic volume, ESVi: indexed end-systolic volume, EF: ejection fraction, GLS: global longitudinal strain, sA: systemic atrium, sAi: indexed systemic atrium, sAS: systemic atrium peak systolic strain, TR: tricuspid regurgitation.

4.2.1 Echocardiographic results

A statistically significant correlation between eRV-EDA and eRV-EDV and between eRV-ESA and eRV-ESV, both as absolute (rho 0.6, p 0.006; rho 0.8, p 0.002) and indexed values (rho 0.8 p 0.007; rho 0.9 p 0.0001) were found.

In addition, we documented a correlation between eRV-EF and FAC and TAPSE (r 0.8, p 0.001 and r 0.7, p 0.03).

Also, E/E' correlated inversely with systemic atrial strain (sAS) (r -0.8, p 0.03).

Lastly, the correlation between sAS and eRV-GLS was also statistically significant (r -0.6, p 0.01).

No statistically significant correlation was found between other echocardiographic data and NYHA class.

4.2.2 CMR results

A significant correlation was found between cRV-EF and cRV-GLS, both endocardial and myocardial (r -0.7, p 0.007, r -0.6, p 0.005).

No statistically significant correlation was found between CMR-derived data and myocardial fibrosis or NYHA class.

4.2.3 Correlation between Echo and CMR results

Among the right ventricle functional parameters assessed, a statistically significant correlation was found between cRV-EDV and cRV-ESV and eRV-EDA and eRV-ESA (r 0.9, p 0.0001; r 0.8, p 0.0001 respectively).

Also, cRV-GLSendo and cRV-GLSmyo correlated significantly with RV-GLS assessed by echocardiography (r 0.8, p 0.001; r 0.7, p 0.01 respectively) and cRV-GLSendo correlated with sAS (r -0.6, p 0.04). These results are shown in *Figure 17*.

No correlation was found between CMR-derived data and other echocardiographic parameters.

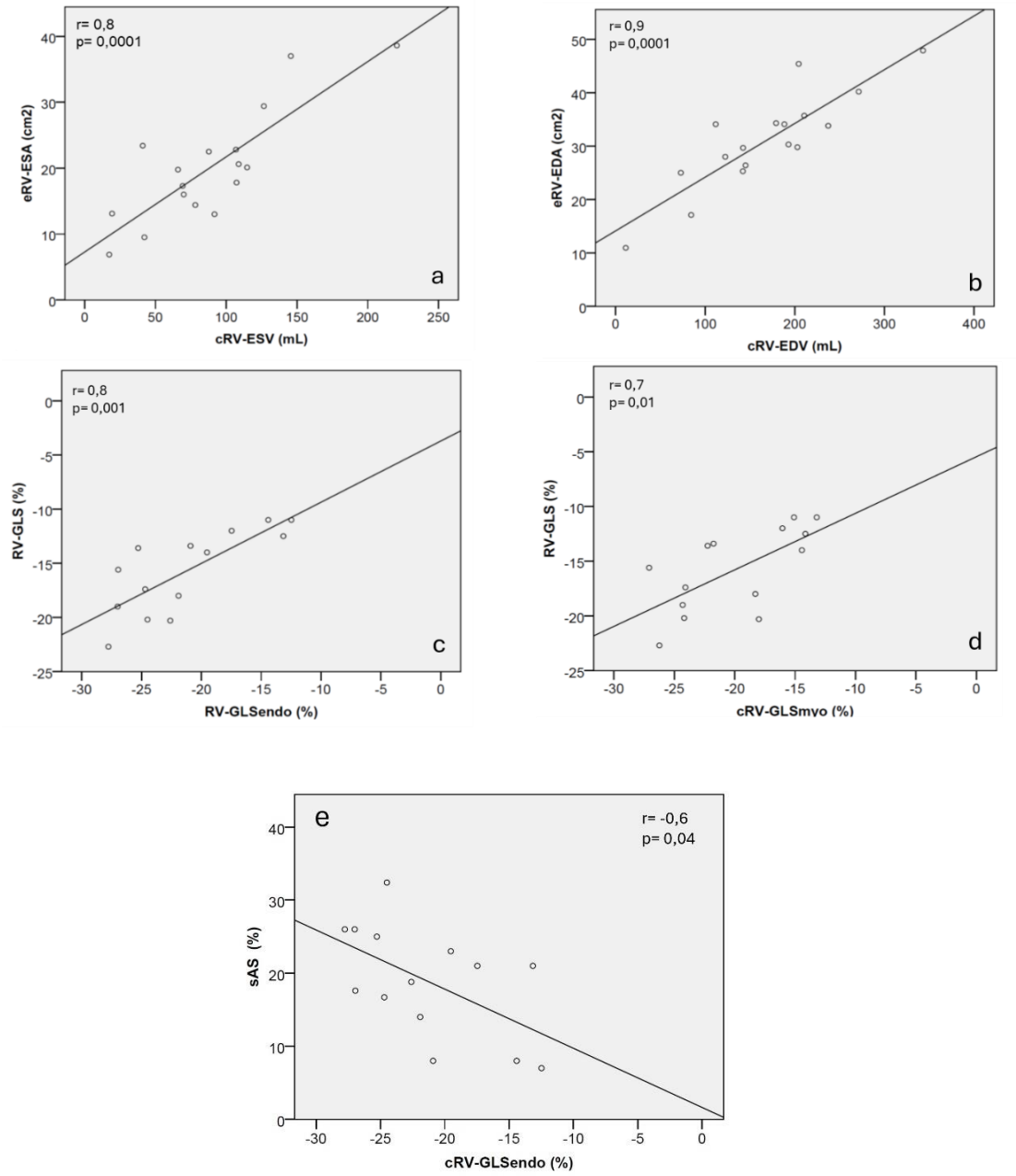

Figure 17- Scatterplot showing the correlation between CMR (x-axis) and Echo (y-axis) derived parameters: cRV-ESV and eRV-ESA (a); cRV-EDV and eRV-EDA (b); cRV-GLS endo, myo and eRV-GLS (c), (d); cRV-GLSendo and sAS (e).

Legend: eRV-ESA: echo-derived right ventricle end-systolic area, cRV-ESV: CMR-derived right ventricle end-systolic volume, eRV-EDA: echo-derived right ventricle end-diastolic area, cRV-EDV: CMR-derived right ventricle end-diastolic volume, RV-GLS: right ventricle global longitudinal strain, cRV-GLSendo: CMR-derived right ventricle endocardial longitudinal strain, cRV-GLSmyo: CMR-derived right ventricle myocardial longitudinal strain, sAS: systemic atrium peak systolic strain.

4.3 CORRELATION BETWEEN CPET AND CARDIAC IMAGING

No correlation was found between CMR imaging parameters and CPET functional data. This result did not change even when evaluating cc-TGA and TGA-Mustard/Senning patients separately.

The only echocardiographic parameter which correlated significantly with peak VO_2 was sAS (r 0.55, p 0.04), *Figure 18*.

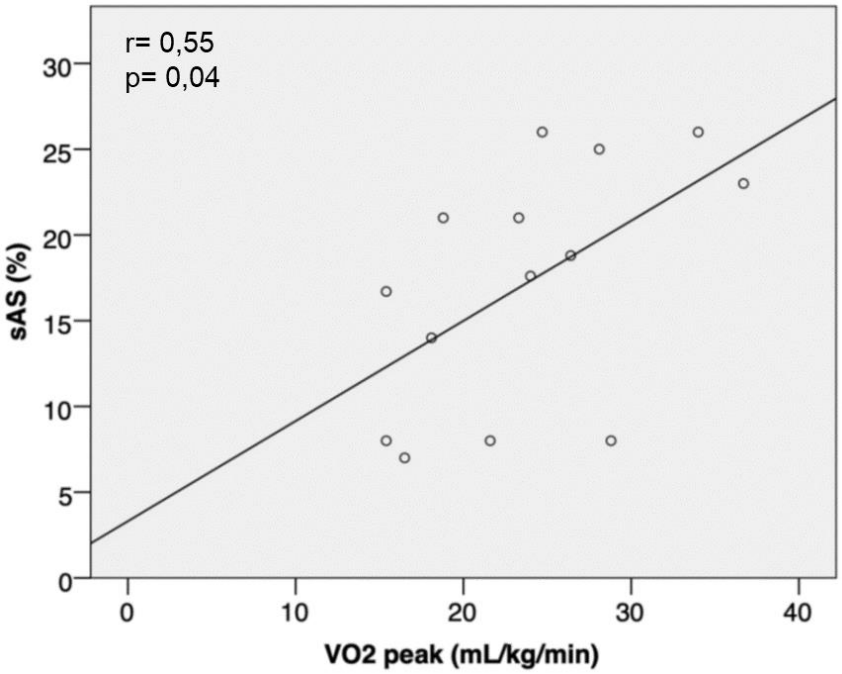

Figure 18- Scatterplot showing the correlation between sAS and Peak VO_2.
Legend: sAS: systemic atrium peak systolic strain, VO2 peak: peak oxygen consumption.

4.4 DIFFERENCES BETWEEN cc-TGA AND D-TGA S/P ATRIAL SWITCH PATIENTS

When cc-TGA and D-TGA patients were compared, the former showed better GLS values as assessed by CMR (cRV-GLSendo -23.2% vs -17.2%, p 0.002; cRV-GLSmyo -21.2% vs -16.7%; p 0.05); and bigger indexed echocardiographic derived systemic atrial area (20.2 cm^2/m^2 vs 8.4 cm^2/m^2, p 0.005). TAPSE values were higher in cc-TGA group (16.2 mm vs 12.2 mm, p 0.04). Also, a trend was noticed towards worse values of sAS in D-TGA (13.8% vs 21.0%, SD 7.6 and 6.9 respectively).

These results are shown in *Figure 19*.

No differences were noticed in terms of tricuspid regurgitation and peak VO_2 between the two populations (D-TGA 22.2 ml/kg/min; ccTGA 25.8 ml/kg/min).

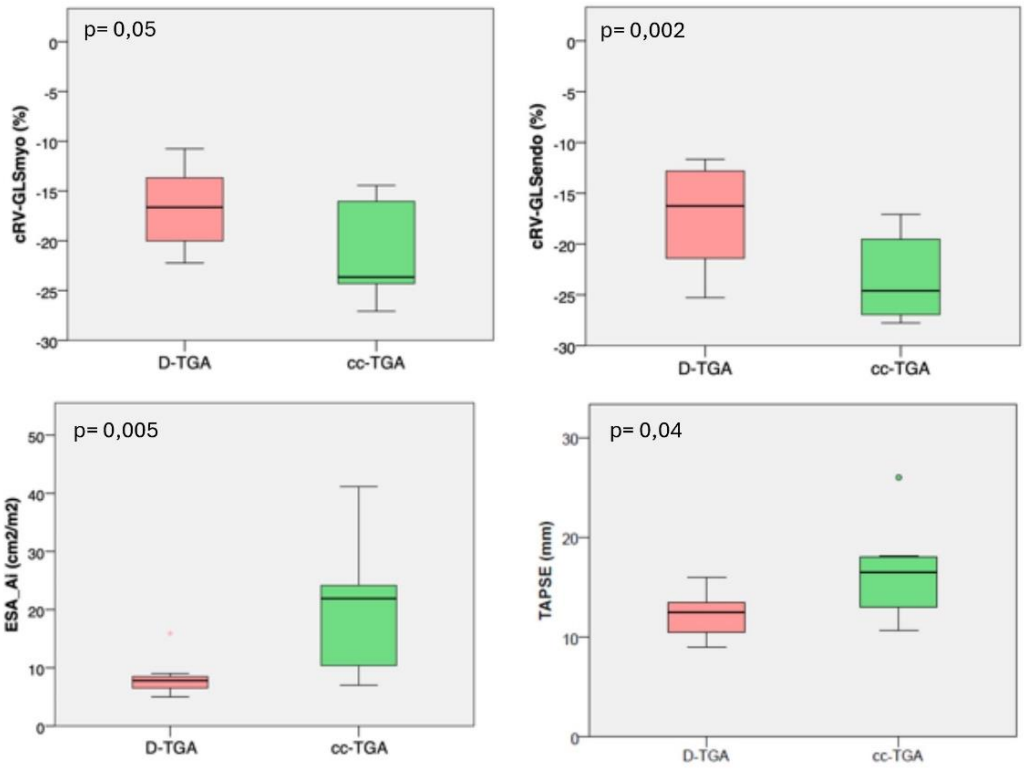

Figure 19- Distribution of cRV-GLS endo and myo, eESA-sAi and TAPSE in the two TGA subgroups.

Legend: cRV-GLSmyo: CMR-derived right ventricle myocardial longitudinal strain, cRV-GLSendo: CMR-derived right ventricle endocardial longitudinal strain, ESA_Ai: indexed echo-derived systemic atrium end-systolic area, TAPSE: tricuspid annular plane systolic excursion.

5 DISCUSSION

To the best of our knowledge, only a few studies compared standard and advanced echocardiographic parameters with CMR parameters and CPET in patients with sRV and biventricular physiologies, sometimes even yielding conflicting results (81).

This study contributes to the limited body of research comparing standard and advanced echocardiographic parameters with CMR parameters and CPET in patients with sRV and biventricular physiologies. Our findings confirm that echocardiography is a well established clinical tool for the clinical follow up of these patients, to evaluate sRV dilatation and to assess systolic function. Also, further investigations of diastolic function in these patients, particularly by assessing atrial strain, may help in better understating the role of diastole in exercise capacity. Lasty, our findings suggest that some differences in terms of cardiac function exists in patients with sRV and different cardiac anatomies.

In this study, a significant correlation was found between 2D echo-derived areas and CMR- derived volumes confirming that 2D echocardiography is a valid first tool to screen right ventricular dilatation, to assess patients longitudinally and to guide the timing for advanced imaging such as CMR. Indeed, CMR remains the gold standard tool to assess sRV, but high costs, lower availability and the need for dedicated skilled staff may limit its use (103).

Three-dimensional echocardiography is an advanced imaging technique that could provide a wealth of information for the evaluation of sRV. Nevertheless, the semi-automated software for 3D analysis needs good quality images, sometimes difficult to achieve when evaluating sRV in TGA population (104). Some studies reported a correlation between echo volumes and CMR volumes (105), (106). This was not identified in our study, but the small sample size may have limited the analysis. Indeed, considering that sRV areas by echocardiography correlated significantly with 3D volumes, we can speculate that with a bigger sample size we might have reached the same result also in comparison with CMR data.

Previous studies demonstrated a good correlation between strain measurements obtained by echocardiography and CMR, and data from our study supports this

finding (107), (108). Also, in this study, a significant correlation was found between sAS and RV-GLS assessed by echo. Impaired atrial function, as it can be in patients after Mustard/Senning operations, can lead to inadequate ventricular filling (109), (110). This may affect firstly ventricular diastolic function and, later, systolic performance. This can potentially lead to decreased cardiac output and, ultimately, heart failure. Thus, monitoring both atrial and ventricular strain parameters longitudinally could provide valuable insights to early identify patients at risk for adverse outcomes and guide treatment strategies (111). In addition, the systematic assessment of atrial strain may help to better understand diastolic function in these patients, which is still poorly understood (112), (70).

The correlation between sAS and peak VO2 may suggest a major role of diastolic function in determining exercise capacity in patients with sRV. The relationship between atrial deformation imaging and peak VO2 has been already investigated in other CHDs (113), (114). By contrast, previous echocardiographic and CMR studies investigated the correlation between functional imaging parameters and CPET in patients with sRV, with no significant results (106), (109). However, atrial deformation imaging was not performed in these studies. Based on the results of the current study we speculate that the presence of pulmonary veins baffle and tricuspid regurgitation can alter atrial compliance and elasticity, especially under exercise, resulting in an insufficient atrial output into sRV.

Lastly, compared to subjects with D-TGA, patients with cc-TGA showed better systolic function, as assessed by CMR-derived GLS values, higher values of TAPSE, systemic atrial area, and a trend toward better values of sAS. These results might be partially explained by the degree of TR, which leads to atrial enlargement and enhance TAPSE values (115), (116).

However, in our study we did not find a difference when comparing the degree of TR among the two subgroups, thus other mechanisms such as altered ventriculo-atrial coupling and issues about atrial contraction may be involved. Ultimately, the absence of atrial surgery could explain the trend toward higher sAS values in cc-TGA group.

5.1 LIMITATIONS

We acknowledge several limitations within our study. Firstly, it is a retrospective, single institution cohort study, thus advanced imaging was not available for all patients.

Specifically, it should be noted that CPET results were available for only 17 out of 19 (89,5%). This is partly due to the fact that CPET is not always feasible in pediatric patients because of the lack of cooperation, and partly because it was not possible to retrieve CPET results conducted outside of the Hospital-University of Padua.

Additionally, there were instances where CMR data or echocardiographic parameters could not be obtained due to limitations associated with the techniques themselves, such as inadequate assessment of cardiac structures in the absence of a good acoustic window. Furthermore, it is important to highlight that echocardiographic and CMR exams were not conducted on the same day, although there was an interval of no more than 12 months between them.

Furthermore, some correlation coefficients are based on a small sample size as measurements were not feasible/available in a considerable number of cases. However, this scenario reflects the practical applicability in everyday clinical practice, as echocardiographic assessment of sRV function is challenging and patients with sRV represent a rare population (117).

6 CONCLUSIONS

In every day clinical practice echocardiogram remains a valid first line tool to assess sRV dimension and function, as well as to guide the timing for advanced imaging modalities such as CMR.

Our study revealed that cc-TGA patients depicted better systolic performance at CMR compared to those with D-TGA population. These findings reflect the peculiar features of cc-TGA population, such as lack of atrial surgery, higher degree of tricuspid regurgitation and the natural history of the disease.

3D echocardiography is a powerful new imaging technique which can provide accurate quantification of functional parameters. Nevertheless, in sRV population 3D echocardiography can be affected by artifacts, poor image quality, and technical issues due to post-processing analysis.

Also, the evaluation of diastolic function in this population is still challenging and poorly understood but, considering the potential implications in term of exercise performance, efforts should be made to provide parameters and cut-off values able to help practitioners in clinical decisions. The investigation of atrial deformation imaging may have a role in this sense.

Similarly, as more patients with sRV are surviving into adulthood, there is a growing need to implement research on this topic by understanding the long-term outcomes to shape the way practitioners approach diagnosis and long-term care of these patients.

7 BIBLIOGRAPHY

1. Sabatino J, Di Salvo G. The new pandemic: ACHD HF. Int J Cardiol. 2022 Jun;356:51–2.

2. Van Der Linde D, Konings EEM, Slager MA, Witsenburg M, Helbing WA, Takkenberg JJM, et al. Birth Prevalence of Congenital Heart Disease Worldwide. J Am Coll Cardiol. 2011 Nov;58(21):2241–7.

3. Foschi M, Di Mauro M, Tancredi F, Capparuccia C, Petroni R, Leonzio L, et al. The Dark Side of the Moon: The Right Ventricle. J Cardiovasc Dev Dis. 2017 Oct 20;4(4):18.

4. Baumgartner H, De Backer J, Babu-Narayan SV, Budts W, Chessa M, Diller GP, et al. 2020 ESC Guidelines for the management of adult congenital heart disease. Eur Heart J. 2021 Feb 11;42(6):563–645.

5. Brida M, Diller GP, Gatzoulis MA. Systemic Right Ventricle in Adults With Congenital Heart Disease: Anatomic and Phenotypic Spectrum and Current Approach to Management. Circulation. 2018 Jan 30;137(5):508–18.

6. Ho SY. Anatomy, echocardiography, and normal right ventricular dimensions. Heart. 2006 Apr 1;92(suppl_1):i2–13.

7. Sanz J, Sánchez-Quintana D, Bossone E, Bogaard HJ, Naeije R. Anatomy, Function, and Dysfunction of the Right Ventricle. J Am Coll Cardiol. 2019 Apr;73(12):1463–82.

8. Kelly RG, Buckingham ME, Moorman AF. Heart Fields and Cardiac Morphogenesis. Cold Spring Harb Perspect Med. 2014 Oct 1;4(10):a015750–a015750.

9. Kiserud T, Acharya G. The fetal circulation. Prenat Diagn. 2004 Dec 30;24(13):1049–59.

10. Molnár AÁ, Sánta A, Merkely B. Echocardiography Imaging of the Right Ventricle: Focus on Three-Dimensional Echocardiography. Diagnostics. 2023 Jul 25;13(15):2470.

11. Naeije R, Badagliacca R. The overloaded right heart and ventricular interdependence. Cardiovasc Res. 2017 Oct 1;113(12):1474–85.

12. Baliga RR, Young JB. Editorial. Heart Fail Clin. 2008 Jul;4(3):xiii–xix.

13. Buckberg G, Hoffman JIE. Right ventricular architecture responsible for mechanical performance: Unifying role of ventricular septum. J Thorac Cardiovasc Surg. 2014 Dec;148(6):3166-3171.e4.

14. Geva T, Powell AJ, Crawford EC, Chung T, Colan SD. Evaluation of Regional Differences in Right Ventricular Systolic Function by Acoustic Quantification Echocardiography and Cine Magnetic Resonance Imaging. Circulation. 1998 Jul 28;98(4):339–45.

15. Roberts WC, Jameson LC, Bahmani A, Roberts CS, Rafael AE, Hall SA. Morphological and Functional Characteristics of the Right Ventricle Functioning as a Systemic Ventricle for Decades After an Atrial Switch Procedure for Complete Transposition of the Great Arteries. Am J Cardiol. 2019 Jun;123(11):1863–7.

16. Valle C, Ujvari A, Elia E, Lu M, Gauthier N, Hoganson D, et al. Right ventricular contraction patterns in healthy children using three-dimensional echocardiography. Front Cardiovasc Med. 2023 Aug 3;10:1141027.

17. Fogel MA, Weinberg PM, Fellows KE, Hoffman EA. A Study in Ventricular–Ventricular Interaction: Single Right Ventricles Compared With Systemic Right Ventricles in a Dual-Chamber Circulation. Circulation. 1995 Jul 15;92(2):219–30.

18. Andrade L, Carazo M, Wu F, Kim Y, Wilson W. Mechanisms for heart failure in systemic right ventricle. Heart Fail Rev. 2020 Jul;25(4):599–607.

19. Pettersen E, Helle-Valle T, Edvardsen T, Lindberg H, Smith HJ, Smevik B, et al. Contraction Pattern of the Systemic Right Ventricle. J Am Coll Cardiol. 2007 Jun;49(25):2450–6.

20. Zong P, Tune JD, Downey HF. Mechanisms of Oxygen Demand/Supply Balance in the Right Ventricle. Exp Biol Med. 2005 Sep;230(8):507–19.

21. Martins P, Castela E. Transposition of the great arteries. Orphanet J Rare Dis. 2008 Dec;3(1):27.

22. Šamánek M, Slavík Z, Zbořilová B, Hroboňová V, Voříšková M, Škovránek J. Prevalence, treatment, and outcome of heart disease in live-born children: A prospective analysis of 91,823 live-born children. Pediatr Cardiol. 1989 Sep;10(4):205–11.

23. Bianca S, Ettore G. Sex ratio imbalance in transposition of the great arteries and possible agricultural environmental risk factors. Images Paediatr Cardiol. 2001 Jul;3(3):10–4.

24. Moorman A. DEVELOPMENT OF THE HEART: (1) FORMATION OF THE CARDIAC CHAMBERS AND ARTERIAL TRUNKS. Heart. 2003 Jul 1;89(7):806–14.

25. Canan A, Ashwath R, Agarwal PP, François C, Rajiah P. Multimodality Imaging of Transposition of the Great Arteries. RadioGraphics. 2021 Mar;41(2):338–60.

26. Warnes CA. Transposition of the Great Arteries. Circulation. 2006 Dec 12;114(24):2699–709.

27. Bevilacqua F, Pasqualin G, Ferrero P, Micheletti A, Negura DG, D'Aiello AF, et al. Overview of Long-Term Outcome in Adults with Systemic Right Ventricle and Transposition of the Great Arteries: A Review. Diagnostics. 2023 Jun 28;13(13):2205.

28. Broberg CS, Van Dissel AC, Minnier J, Aboulhosn J, Kauling RM, Ginde S, et al. Long-Term Outcomes After Atrial Switch Operation for Transposition of the Great Arteries. J Am Coll Cardiol. 2022 Sep;80(10):951–63.

29. Cuypers JAAE, Eindhoven JA, Slager MA, Opi P, Utens EMWJ, Helbing WA, et al. The natural and unnatural history of the Mustard procedure: long-term outcome up to 40 years. Eur Heart J. 2014 Jul 1;35(25):1666–74.

30. Konstantinov IE, Alexi-Meskishvili VV, Williams WG, Freedom RM, Van Praagh R. Atrial switch operation: past, present, and future. Ann Thorac Surg. 2004 Jun;77(6):2250–8.

31. Gaur L, Cedars A, Diller GP, Kutty S, Orwat S. Management considerations in the adult with surgically modified d-transposition of the great arteries. Heart. 2021 Oct;107(20):1613–9.

32. Khairy P, Landzberg MJ, Lambert J, O'Donnell CP. Long-term outcomes after the atrial switch for surgical correction of transposition: a meta-analysis comparing the Mustard and Senning procedures. Cardiol Young. 2004 Jun;14(3):284–92.

33. Gelatt M, Hamilton RM, McCrindle BW, Connelly M, Davis A, Harris L, et al. Arrhythmia and Mortality After the Mustard Procedure: A 30-Year Single-Center Experience. J Am Coll Cardiol. 1997 Jan;29(1):194–201.

34. Diller GP. Chasing a moving target: outcome and risk stratification in patients with transposition of the great arteries after atrial switch operation. Eur Heart J. 2014 Jul 1;35(25):1637–41.

35. Brida M, Lovrić D, Griselli M, Riesgo Gil F, Gatzoulis MA. Heart failure in adults with congenital heart disease. Int J Cardiol. 2022 Jun;357:39–45.

36. Yehya A, Lyle T, Pernetz MA, McConnell ME, Kogon B, Book WM. Pulmonary arterial hypertension in patients with prior atrial switch procedure for d-transposition of great arteries (dTGA). Int J Cardiol. 2010 Sep;143(3):271–5.

37. Auer J, Pujol C, Maurer SJ, Nagdyman N, Ewert P, Tutarel O. Congenitally Corrected Transposition of the Great Arteries in Adults—A Contemporary Single Center Experience. J Cardiovasc Dev Dis. 2021 Sep 15;8(9):113.

38. Amaral F, Valente AM, Manso PH, Gali LG, Braggion-Santos MF, Rocha JM, et al. Congenitally Corrected Transposition of the Great Arteries in the Adult. Braz J Cardiovasc Surg [Internet]. 2022 [cited 2024 Feb 29];37(4). Available from: https://cdn.publisher.gn1.link/bjcvs.org/pdf/v37n4a16.pdf

39. Shiraishi I. Basic and Comprehensive Outlines of Cardiovascular Embryology and Morphogenesis [Internet]. Japanese Society of Pediatric Cardiology and Cardiac Surgery; 2020 [cited 2024 May 25]. Available from: https://doi.org/10.24509/jpccs.19-015

40. Smood B, Kirklin JK, Pavnica J, Tresler M, Johnson WH, Cleveland DC, et al. Congenitally Corrected Transposition Presenting in the First Year of Life:

Survival and Fate of the Systemic Right Ventricle. World J Pediatr Congenit Heart Surg. 2019 Jan;10(1):42–9.

41. Graham TP, Bernard YD, Mellen BG, Celermajer D, Baumgartner H, Cetta F, et al. Long-term outcome in congenitally corrected transposition of the great arteries. J Am Coll Cardiol. 2000 Jul;36(1):255–61.

42. Huhta JC, Maloney JD, Ritter DG, Ilstrup DM, Feldt RH. Complete atrioventricular block in patients with atrioventricular discordance. Circulation. 1983 Jun;67(6):1374–7.

43. Hauser M. Impaired myocardial blood flow and coronary flow reserve of the anatomical right systemic ventricle in patients with congenitally corrected transposition of the great arteries. Heart. 2003 Oct 1;89(10):1231–5.

44. Carazo M, Andrade L, Kim Y, Wilson W, Wu FM. Assessment and management of heart failure in the systemic right ventricle. Heart Fail Rev. 2020 Jul;25(4):609–21.

45. Karamlou T, Devlin PJ, Hammoud MS. Late Systemic Right Ventricle Failure. J Am Coll Cardiol. 2022 Sep;80(10):964–6.

46. Kostura M, Smalley C, Koyfman A, Long B. Right heart failure: A narrative review for emergency clinicians. Am J Emerg Med. 2022 Aug;58:106–13.

47. Ciuca C, Balducci A, Angeli E, Di Dio M, Assenza GE, Mariucci E, et al. Long Term Follow-Up of Patients with Systemic Right Ventricle and Biventricular Physiology: A Single Centre Experience. J Cardiovasc Dev Dis. 2023 May 17;10(5):219.

48. Theissen P, Kaemmerer H, Sechtem U, Luhmer I, Smolarz K, Kallfelz H, et al. Magnetic Resonance Imaging of Cardiac Function and Morphology in Patients with Transposition of the Great Arteries Following Mustard Procedure. Thorac Cardiovasc Surg. 1991 Dec;39(S 3):221–4.

49. Gordon B, González-Fernández V, Dos-Subirà L. Myocardial fibrosis in congenital heart disease. Front Pediatr. 2022 Nov 18;10:965204.

50. Babu-Narayan SV, Goktekin O, Moon JC, Broberg CS, Pantely GA, Pennell DJ, et al. Late Gadolinium Enhancement Cardiovascular Magnetic Resonance of the Systemic Right Ventricle in Adults With Previous Atrial Redirection Surgery for Transposition of the Great Arteries. Circulation. 2005 Apr 26;111(16):2091–8.

51. Pavsic N, Zbacnik R, Berden P, Kacar P, Dolenc J, Stalc M, et al. The association between myocardial ischemia and myocardial dysfunction in adult patients with systemic right ventricle – A single centre multimodality study. Int J Cardiol. 2023 Aug;384:31–6.

52. Lewis M, Ginns J, Rosenbaum M. Is systemic right ventricular function by cardiac MRI related to the degree of tricuspid regurgitation in congenitally corrected transposition of the great arteries? Int J Cardiol. 2014 Jul;174(3):586–9.

53. Silini A, Avesani M, Houyel L, Thambo JB, Iriart X. The pivotal role of tricuspid regurgitation in the failing systemic right ventricle: The “chicken and egg story”. Arch Cardiovasc Dis. 2022 Aug;115(8–9):476–86.

54. Prieto LR, Hordof AJ, Secic M, Rosenbaum MS, Gersony WM. Progressive Tricuspid Valve Disease in Patients With Congenitally Corrected Transposition of the Great Arteries. Circulation. 1998 Sep 8;98(10):997–1005.

55. Fuller S. Comparing Long-Term Sequelae of the Systemic Right Ventricle: An Overview of Single Versus Biventricular Arrangements. Semin Thorac Cardiovasc Surg Pediatr Card Surg Annu. 2022;25:2–10.

56. Rog B, Salapa K, Okolska M, Dluzniewska N, Werynski P, Podolec P, et al. Clinical Evaluation of Exercise Capacity in Adults with Systemic Right Ventricle. Tex Heart Inst J. 2019 Feb 1;46(1):14–20.

57. Hahn RT, Lerakis S, Delgado V, Addetia K, Burkhoff D, Muraru D, et al. Multimodality Imaging of Right Heart Function. J Am Coll Cardiol. 2023 May;81(19):1954–73.

58. Shiina Y, Inai K, Takahashi T, Taniguchi K, Watanabe E, Fukushima K, et al. Inter- and intra-ventricular dyssynchrony in the systemic right ventricle is a surrogate marker of major cardiac events in mildly symptomatic patients. Heart Vessels. 2018 Sep;33(9):1086–93.

59. Di Salvo G, Miller O, Babu Narayan S, Li W, Budts W, Valsangiacomo Buechel ER, et al. Imaging the adult with congenital heart disease: a multimodality imaging approach—position paper from the EACVI. Eur Heart J - Cardiovasc Imaging. 2018 Oct 1;19(10):1077–98.

60. Iriart X, Roubertie F, Jalal Z, Thambo JB. Quantification of systemic right ventricle by echocardiography. Arch Cardiovasc Dis. 2016 Feb;109(2):120–7.

61. Chen-Tournoux A, Therrien J, Afilalo J. Echocardiographic Strain Imaging in the Systemic Right Ventricle: Early Clue for Late Decompensation. Can J Cardiol. 2020 Sep;36(9):1341–3.

62. Lissin LW, Li W, Murphy DJ, Hornung T, Swan L, Mullen M, et al. Comparison of transthoracic echocardiography versus cardiovascular magnetic resonance imaging for the assessment of ventricular function in adults after atrial switch procedures for complete transposition of the great arteries. Am J Cardiol. 2004 Mar;93(5):654–7.

63. Zaidi A, Knight DS, Augustine DX, Harkness A, Oxborough D, Pearce K, et al. Echocardiographic Assessment of the Right Heart in Adults: A Practical Guideline from the British Society of Echocardiography. Echo Res Pract. 2020 Mar;7(1):G19–41.

64. Rudski LG, Lai WW, Afilalo J, Hua L, Handschumacher MD, Chandrasekaran K, et al. Guidelines for the Echocardiographic Assessment of the Right Heart in Adults: A Report from the American Society of Echocardiography. J Am Soc Echocardiogr. 2010 Jul;23(7):685–713.

65. Lang RM, Badano LP, Mor-Avi V, Afilalo J, Armstrong A, Ernande L, et al. Recommendations for Cardiac Chamber Quantification by Echocardiography in Adults: An Update from the American Society of Echocardiography and the European Association of Cardiovascular Imaging. J Am Soc Echocardiogr. 2015 Jan;28(1):1-39.e14.

66. Derrick GP. Abnormalities of right ventricular long axis function after atrial repair of transposition of the great arteries. Heart. 2001 Aug 1;86(2):203–6.

67. DiLorenzo MP, Bhatt SM, Mercer-Rosa L. How best to assess right ventricular function by echocardiography. Cardiol Young. 2015 Dec;25(8):1473–81.

68. Lipczyńska M, Szymański P, Kumor M, Klisiewicz A, Mazurkiewicz Ł, Hoffman P. Global Longitudinal Strain May Identify Preserved Systolic Function of the Systemic Right Ventricle. Can J Cardiol. 2015 Jun;31(6):760–6.

69. Jung YH, Ren X, Suffredini G, Dodd-o JM, Gao WD. Right ventricular diastolic dysfunction and failure: a review. Heart Fail Rev. 2022 Jul;27(4):1077–90.

70. Ta HT, Alsaied T, Steele JM, Truong VT, Mazur W, Nagueh SF, et al. Atrial Function and Its Role in the Non-invasive Evaluation of Diastolic Function in Congenital Heart Disease. Pediatr Cardiol. 2020 Apr;41(4):654–68.

71. Reich O, Ruth C, Marek J. Long term ventricular performance after intra-atrial correction of transposition: left ventricular filling is the major limitation. Heart. 1997 Oct 1;78(4):376–81.

72. Mavrogeni SI. CMR of the right ventricle. Toward a better understanding of the dark side of the moon. Hellenic J Cardiol. 2020 Mar;61(2):118–9.

73. Grothues F, Moon JC, Bellenger NG, Smith GS, Klein HU, Pennell DJ. Interstudy reproducibility of right ventricular volumes, function, and mass with cardiovascular magnetic resonance. Am Heart J. 2004 Feb;147(2):218–23.

74. Lebherz C, Gerhardus M, Lammers AE, Helm P, Tutarel O, Bauer U, et al. Late outcome, therapy and systemic ventricular function in patients with a systemic right ventricle: data of the German National Register for Congenital Heart Defects. Cardiol Young. 2022 Aug;32(8):1235–45.

75. Aarsvold KJ, Danford DA, Yetman AT. Oxygen Uptake Efficiency Slope Predicts Adverse Outcome Following Atrial Switch Procedure. Pediatr Cardiol. 2022 Mar;43(3):561–6.

76. Diller GP, Dimopoulos K, Okonko D, Li W, Babu-Narayan SV, Broberg CS, et al. Exercise Intolerance in Adult Congenital Heart Disease: Comparative Severity, Correlates, and Prognostic Implication. Circulation. 2005 Aug 9;112(6):828–35.

77. Gavotto A, Abassi H, Rola M, Serrand C, Picot MC, Iriart X, et al. Factors associated with exercise capacity in patients with a systemic right ventricle. Int J Cardiol. 2019 Oct;292:230–5.

78. Ladouceur M, Kachenoura N, Soulat G, Bollache E, Redheuil A, Azizi M, et al. Impaired atrioventricular transport in patients with transposition of the great arteries palliated by atrial switch and preserved systolic right ventricular function: A magnetic resonance imaging study: LADOUCEUR et al. Congenit Heart Dis. 2017 Jul;12(4):458–66.

79. Das BB, Godoy A, Kadish T, Niu J. Maximal versus sub-maximal effort during cardiopulmonary exercise testing in adults with congenital heart disease: outcome analysis of short-term cardiac-related events. Cardiol Young. 2021 Jan;31(1):91–6.

80. Driscoll D. Ventilatory Efficiency and Aerobic Capacity Predict Event-Free Survival in Adults With Atrial Repair for Complete Transposition of the Great Arteries. J Am Coll Cardiol. 2009 Apr;53(17):1556–7.

81. Helsen F, De Meester P, Van De Bruaene A, Gabriels C, Santens B, Claeys M, et al. Right ventricular systolic dysfunction at rest is not related to decreased exercise capacity in patients with a systemic right ventricle. Int J Cardiol. 2018 Jun;260:66–71.

82. Li W, Hornung TS, Francis DP, O'Sullivan C, Duncan A, Gatzoulis M, et al. Relation of Biventricular Function Quantified by Stress Echocardiography to Cardiopulmonary Exercise Capacity in Adults With Mustard (Atrial Switch) Procedure for Transposition of the Great Arteries. Circulation. 2004 Sep 14;110(11):1380–6.

83. Gonçalves AV, Mano T, Agapito A, Rosa SA, De Sousa L, Rio P, et al. Prognostic power of anaerobic threshold parameters in patients with transposition of the great arteries and systemic right ventricle. Cardiol Young. 2019 Dec;29(12):1445–51.

84. Santens B, Van De Bruaene A, De Meester P, D'Alto M, Reddy S, Bernstein D, et al. Diagnosis and treatment of right ventricular dysfunction in congenital heart disease. Cardiovasc Diagn Ther. 2020 Oct;10(5):1625–45.

85. Skoglund K, Heimdahl J, Mandalenakis Z, Thilén U, Johansson B, Christersson C, et al. Effect of medical treatment in patients with systemic right ventricle. Scand Cardiovasc J. 2020 Sep 2;54(5):300–5.

86. Sabbah BN, Arabi TZ, Shafqat A, Abdul Rab S, Razak A, Albert-Brotons DC. Heart failure in systemic right ventricle: Mechanisms and therapeutic options. Front Cardiovasc Med. 2023 Jan 10;9:1064196.

87. Andersen S, Andersen A, Nielsen-Kudsk JE. The renin–angiotensin–aldosterone-system and right heart failure in congenital heart disease. IJC Heart Vasc. 2016 Jun;11:59–65.

88. Dos L, Pujadas S, Estruch M, Mas A, Ferreira-González I, Pijuan A, et al. Eplerenone in systemic right ventricle: Double blind randomized clinical trial. The evedes study. Int J Cardiol. 2013 Oct;168(6):5167–73.

89. Van Der Bom T, Winter MM, Bouma BJ, Groenink M, Vliegen HW, Pieper PG, et al. Effect of Valsartan on Systemic Right Ventricular Function: A Double-Blind, Randomized, Placebo-Controlled Pilot Trial. Circulation. 2013 Jan 22;127(3):322–30.

90. Nederend M, Kiès P, Regeer MV, Vliegen HW, Mertens BJ, Robbers-Visser D, et al. Tolerability and beneficial effects of sacubitril/valsartan on systemic right ventricular failure. Heart. 2023 Oct;109(20):1525–32.

91. Fusco F, Scognamiglio G, Merola A, Iannuzzi A, Palma M, Grimaldi N, et al. Safety and Efficacy of Sacubitril/Valsartan in Patients With a Failing Systemic Right Ventricle: A Prospective Single-Center Study. Circ Heart Fail. 2022 Dec 2;e009848.

92. Iriart X, Horovitz A, Van Geldorp IE, Barnetche T, Lederlin M, De Guillebon M, et al. The role of echocardiography in the assessment of right ventricular systolic function in patients with transposition of the great arteries and atrial redirection. Arch Cardiovasc Dis. 2012 Aug;105(8–9):432–41.

93. Obokata M, Nagata Y, Wu VCC, Kado Y, Kurabayashi M, Otsuji Y, et al. Direct comparison of cardiac magnetic resonance feature tracking and 2D/3D echocardiography speckle tracking for evaluation of global left ventricular strain. Eur Heart J – Cardiovasc Imaging. 2016 May;17(5):525–32.

94. Samyn MM, Yan K, Masterson C, Goot BH, Saudek D, Lavoie J, et al. Echocardiography vs cardiac magnetic resonance imaging assessment of the systemic right ventricle for patients with d-transposition of the great arteries status post atrial switch. Congenit Heart Dis. 2019 Nov;14(6):1138–48.

95. Sabatino J, Di Salvo G, Krupickova S, Fraisse A, Prota C, Bucciarelli V, et al. Left Ventricular Twist Mechanics to Identify Left Ventricular Noncompaction in Childhood. Circ Cardiovasc Imaging. 2019 Apr;12(4):e007805.

96. Prota C, Di Salvo G, Sabatino J, Josen M, Paredes J, Sirico D, et al. Prognostic value of echocardiographic parameters in pediatric patients with Ebstein's anomaly. Int J Cardiol. 2019 Mar;278:76–83.

97. Fratz S, Chung T, Greil GF, Samyn MM, Taylor AM, Valsangiacomo Buechel ER, et al. Guidelines and protocols for cardiovascular magnetic resonance in children and adults with congenital heart disease: SCMR expert consensus group on congenital heart disease. J Cardiovasc Magn Reson Off J Soc Cardiovasc Magn Reson. 2013 Jun 13;15(1):51.

98. Fogel MA, Anwar S, Broberg C, Browne L, Chung T, Johnson T, et al. Society for Cardiovascular Magnetic Resonance/European Society of Cardiovascular Imaging/American Society of Echocardiography/Society for Pediatric Radiology/North American Society for Cardiovascular Imaging Guidelines for the Use of Cardiac Magnetic Resonance in Pediatric Congenital and Acquired Heart Disease: Endorsed by The American Heart Association. Circ

Cardiovasc Imaging [Internet]. 2022 Jun [cited 2024 May 9];15(6). Available from: https://www.ahajournals.org/doi/10.1161/CIRCIMAGING.122.014415

99. Gregov A, Hrabak Paar M. Magnetic Resonance Imaging Assessment of Right Ventricular Deformation in Patients With Transposition of the Great Arteries. J Thorac Imaging. 2022 Nov;37(6):W85–91.

100. Morais P, Marchi A, Bogaert JA, Dresselaers T, Heyde B, D'hooge J, et al. Cardiovascular magnetic resonance myocardial feature tracking using a non-rigid, elastic image registration algorithm: assessment of variability in a real-life clinical setting. J Cardiovasc Magn Reson. 2016 Dec;19(1):24.

101. Rajiah PS, Kalisz K, Broncano J, Goerne H, Collins JD, François CJ, et al. Myocardial Strain Evaluation with Cardiovascular MRI: Physics, Principles, and Clinical Applications. RadioGraphics. 2022 Jul;42(4):968–90.

102. Scatteia A, Baritussio A, Bucciarelli-Ducci C. Strain imaging using cardiac magnetic resonance. Heart Fail Rev. 2017 Jul;22(4):465–76.

103. Samyn MM, Yan K, Masterson C, Goot BH, Saudek D, Lavoie J, et al. Echocardiography vs cardiac magnetic resonance imaging assessment of the systemic right ventricle for patients with d-transposition of the great arteries status post atrial switch. Congenit Heart Dis. 2019 Nov;14(6):1138–48.

104. Molnár AÁ, Sánta A, Merkely B. Echocardiography Imaging of the Right Ventricle: Focus on Three-Dimensional Echocardiography. Diagnostics. 2023 Jul 25;13(15):2470.

105. Kutty S, Li L, Polak A, Gribben P, Danford DA. Echocardiographic Knowledge-Based Reconstruction for Quantification of the Systemic Right Ventricle in Young Adults With Repaired D-Transposition of Great Arteries. Am J Cardiol. 2012 Mar;109(6):881–8.

106. Schneider M, Beichl M, Nietsche C, Beitzke D, Porenta G, Beran G, et al. Systematic Evaluation of Systemic Right Ventricular Function. J Clin Med. 2019 Dec 31;9(1):107.

107. Obokata M, Nagata Y, Wu VCC, Kado Y, Kurabayashi M, Otsuji Y, et al. Direct comparison of cardiac magnetic resonance feature tracking and 2D/3D echocardiography speckle tracking for evaluation of global left ventricular strain. Eur Heart J – Cardiovasc Imaging. 2016 May;17(5):525–32.

108. Claus P, Omar AMS, Pedrizzetti G, Sengupta PP, Nagel E. Tissue Tracking Technology for Assessing Cardiac Mechanics. JACC Cardiovasc Imaging. 2015 Dec;8(12):1444–60.

109. Franzoso FD, Wohlmuth C, Greutmann M, Kellenberger CJ, Oxenius A, Voser EM, et al. Atrial Function after the Atrial Switch Operation for Transposition of the Great Arteries: Comparison with Arterial Switch and Normals by Cardiovascular Magnetic Resonance. Congenit Heart Dis. 2016 Sep;11(5):426–36.

110. Gaynor SL, Maniar HS, Prasad SM, Steendijk P, Moon MR. Reservoir and conduit function of right atrium: impact on right ventricular filling and cardiac output. Am J Physiol-Heart Circ Physiol. 2005 May;288(5):H2140–5.

111. Dorobantu DM, Amir NH, Wadey CA, Sharma C, Stuart AG, Williams CA, et al. The Role of Speckle-Tracking Echocardiography in Predicting Mortality and Morbidity in Patients With Congenital Heart Disease: A Systematic Review and Meta-analysis. J Am Soc Echocardiogr Off Publ Am Soc Echocardiogr. 2024 Feb;37(2):216–25.

112. Gaynor SL, Maniar HS, Bloch JB, Steendijk P, Moon MR. Right Atrial and Ventricular Adaptation to Chronic Right Ventricular Pressure Overload. Circulation [Internet]. 2005 Aug 30 [cited 2024 May 8];112(9_supplement). Available from: https://www.ahajournals.org/doi/10.1161/CIRCULATIONAHA.104.517789

113. Avesani M, Borrelli N, Krupickova S, Sabatino J, Donne GD, Ibrahim A, et al. Echocardiography and cardiac magnetic resonance in children with repaired tetralogy of Fallot: New insights in cardiac mechanics and exercise capacity. Int J Cardiol. 2020 Dec;321:144–9.

114. Rato J, Mendes SC, Sousa A, Lemos M, Martins DS, Anjos R. The Influence of Atrial Strain on Functional Capacity in Patients with the Fontan Circulation. Pediatr Cardiol. 2020 Dec;41(8):1730–8.

115. Silini A, Avesani M, Houyel L, Thambo JB, Iriart X. The pivotal role of tricuspid regurgitation in the failing systemic right ventricle: The “chicken and egg story”. Arch Cardiovasc Dis. 2022 Aug;115(8–9):476–86.

116. Muraru D, Badano LP, Hahn RT, Lang RM, Delgado V, Wunderlich NC, et al. Atrial secondary tricuspid regurgitation: pathophysiology, definition, diagnosis, and treatment. Eur Heart J. 2024 Mar 14;45(11):895–911.

117. Marelli AJ, Ionescu-Ittu R, Mackie AS, Guo L, Dendukuri N, Kaouache M. Lifetime Prevalence of Congenital Heart Disease in the General Population From 2000 to 2010. Circulation. 2014 Aug 26;130(9):749–56.